HDL-TR-1800

AD A040111

Investigations into the Causes of Vacuum Degradation in a Ceramic-to-Metal Seal Vacuum Tube

MAY 1977

U.S. Army Materiel Development and Readiness Command
HARRY DIAMOND LABORATORIES
Adelphi, Maryland 20783

TR-1800—*Investigations into the Causes of Vacuum Degradation in a Ceramic-to-Metal Seal Vacuum Tube*—by William K. McNeil

The findings in this report are not to be construed as an official Department of the Army position unless so designated by other authorized documents.

Citation of manufacturers' or trade names does not constitute an official indorsement or approval of the use thereof.

Destroy this report when it is no longer needed. Do not return it to the originator.

UNCLASSIFIED

SECURITY CLASSIFICATION OF THIS PAGE (When Data Entered)

REPORT DOCUMENTATION PAGE

READ INSTRUCTIONS BEFORE COMPLETING FORM

1. REPORT NUMBER: HDL-TR-1808	2. GOVT ACCESSION NO.
3. RECIPIENT'S CATALOG NUMBER	
4. TITLE (and Subtitle): Investigations into the Causes of Vacuum Degradation in a Ceramic-to-Metal Seal Vacuum Tube.	5. TYPE OF REPORT & PERIOD COVERED: Technical Report.
	6. PERFORMING ORG. REPORT NUMBER
7. AUTHOR(s): William K. McNeil	8. CONTRACT OR GRANT NUMBER(s)
9. PERFORMING ORGANIZATION NAME AND ADDRESS: Harry Diamond Laboratories, 2800 Powder Mill Road, Adelphi, MD 20783	10. PROGRAM ELEMENT, PROJECT, TASK AREA & WORK UNIT NUMBERS: DA: 1X222251D231, Program Ele: 2.22.51A
11. CONTROLLING OFFICE NAME AND ADDRESS: Commander, Picatinny Arsenal, Dover, NJ 07801	12. REPORT DATE: May 77
	13. NUMBER OF PAGES: 49
14. MONITORING AGENCY NAME & ADDRESS(if different from Controlling Office)	15. SECURITY CLASS. (of this report): Unclassified
	15a. DECLASSIFICATION/DOWNGRADING SCHEDULE: NA

16. DISTRIBUTION STATEMENT (of this Report)

Approved for public release; distribution unlimited.

17. DISTRIBUTION STATEMENT (of the abstract entered in Block 20, if different from Report)

18. SUPPLEMENTARY NOTES

HDL Project: 719577
DRCMS Code: 2200.2..EN028X1

19. KEY WORDS (Continue on reverse side if necessary and identify by block number)

Diffusion	Desorption
Outgassing	Quadrupole gas analyzer
Ceramic microcracking	Acoustic emissions
Thoriated tungsten filaments	Torr diatomic
Gas flow rate	Porosity vacuum envelope

20. ABSTRACT (Continue on reverse side if necessary and identify by block number)

The root causes are explored for vacuum degradation in a vacuum tube ("bottle") that is constituted of a stacked assembly of alternately arranged metal and high alumina ceramic members. Vacuum degradation caused by leaking, permeation, or outgassing was investigated. Leaking, as a serious failure mode, was eliminated early in the investigation after it was determined that in failed items the ambient gases were predominately nitrogen and hydrogen and there was no oxygen. Additionally, the rate of change of gas

DD FORM 1 JAN 73 1473 EDITION OF 1 NOV 65 IS OBSOLETE

UNCLASSIFIED

SECURITY CLASSIFICATION OF THIS PAGE (When Data Entered)

pressure with time for failed assemblies was orders of magnitude less than that of any known real leak. Hydrogen was assumed to have entered the vacuum space via permeation, but exhaustive experimental and theoretical evidence revealed that niobium was the most permeable material in the vacuum envelope. However, permeation rates on vacuum bottles containing niobium yield storage life expectancies in excess of 20 yr. Data presented establish that a primary A2 failure mode is one in which microcracks through the ceramic intersect gas-filled pores (mostly nitrogen) and permit gas to degrade the vacuum. Additionally, thoriated tungsten filaments getter hydrogen gas at one time and after a diffusion lag time release this hydrogen into the vacuum space.

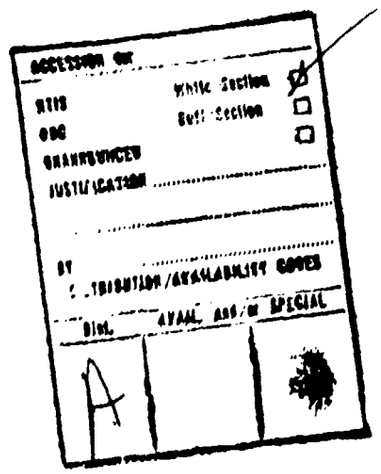

CONTENTS

CONTENTS (Cont'd)

FIGURES

FIGURES (Cont'd)

TABLES

1. INTRODUCTION

The Army has many requirements for vacuum tubes ("bottles") employing ceramic-to-metal sealing techniques. The vacuum tube that this report concerns (fig. 1) includes an envelope constituted of a stacked assembly of alternately arranged metal and ceramic members. Some of the metal members serve as electrical terminals, and the ceramic members serve as insulative spaces between the metal members. One end of the envelope is completed by a composite end member that is separated from the anode terminal by a ceramic cylinder. The cylinder comprises a centrally bored metal cap in which the cold cathode (nonemitting) is fitted and bonded. The other end of the envelope is completed by a ceramic disk that supports the hot cathode or electron emitter.

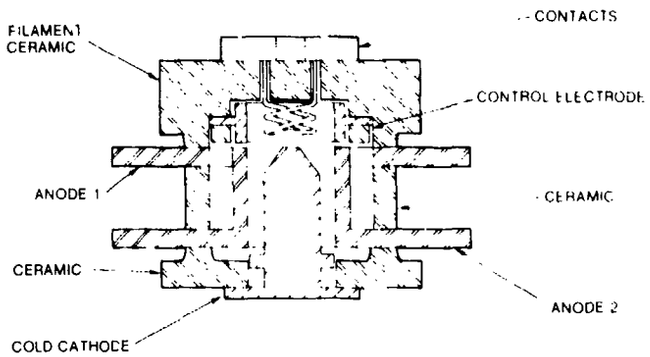

Figure 1. Basic A2 vacuum envelope.

In one of these requirements, the power supply, vacuum tube, and modulator are interconnected. As can be seen from figure 2, points E_1 or E_3 shorted to ground cause capacitor C7, charged to 1200 V, to be connected essentially across the collector-to-emitter junction of transistor Q_3.

The corresponding transistor overload results in an open or short-circuited Q_3, depending on whether the duration of the short circuit is greater or less than 50 μs.

The first Q_3 failure was reported in November 1964 at the Harry Diamond Laboratories (HDL). The accompanying failure analysis report attributed this failure to a high-voltage arc in the power supply. That report established no reason for this arc. It was characteristic of the failure of Q_3 that after it was replaced there was no subsequent failure. During the next several years, there were occasional Q_3 failures, which were attributed to test operator carelessness, thermal overload of Q_3, high voltage arcing in the power supply, or arcing in gassy tubes. Fixes were incorporated to reduce the thermal

stress of Q_3, and work procedures were incorporated to preclude test-operator carelessness. But Q_3 failures continued at an acceptably low rate until December 1972 when the rate increased significantly.

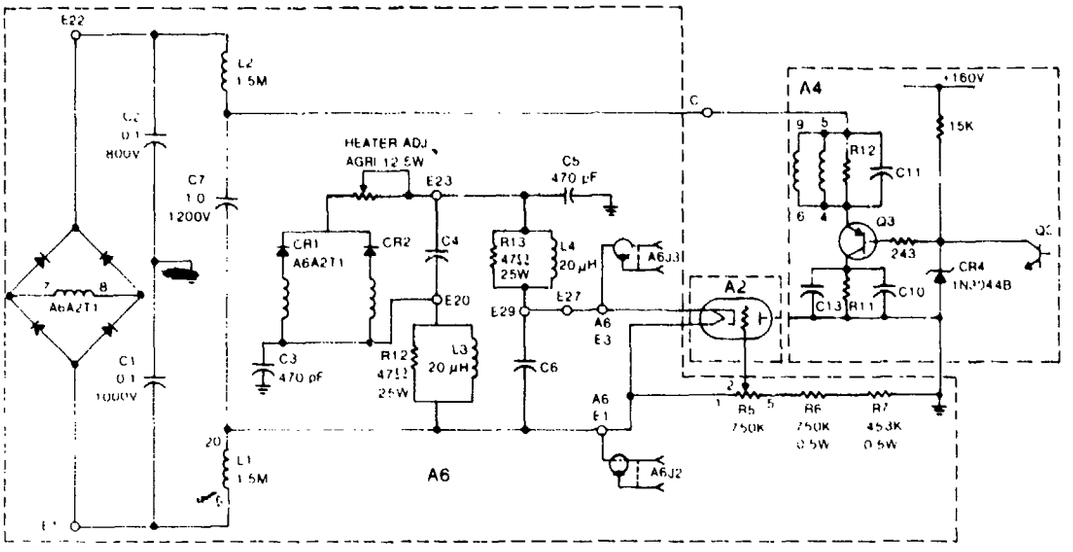

Figure 2. Interconnecting diagram.

In April 1973, HDL established a failure-analysis team to determine the root cause of Q_3 failures and to recommend appropriate corrective actions to prevent future failures. The failure-analysis team issued three interim reports.

Interim report No. 1 (26 April 1973) established that the source of energy for all Q_3 failures was capacitor A3C7 in the power supply. This capacitor could be discharged through Q_3 by an arc in the A2 vacuum tube, a short circuit in the wiring harness, or a short circuit in the high-voltage circuit of the power supply.

Interim Report No. 2 (3 July 1973) concluded that there were three candidates for causing arcing:

a. Flakes, metal plating, metal chips, or metal slivers getting into or near the open A6J2 or A6J3 filament test jacks and causing the high-voltage line to arc to ground

b. A gassy or contaminated A2

c. An initial arc from the rotor of the A6A3R5 grid potentiometer to ground through the adjustment screw and a secondary arc from the high-voltage terminal of A6A3R5 to the rotor

Interim Report No. 3 (24 January 1974) described the following results:

a. Many old tubes were connected in a circuit, similar to that in figure 2. The arcing of some tubes caused Q3 failures identical to those previously reported.

b. An ion current measuring system was developed that could determine the quality of the tube vacuum.

c. Tubes from units that had previously experienced Q_3 failure were measured on the HDL ion current meter, and all showed excessive ion current levels.

d. It was established that gassy A2's were responsible for most, if not all, Q_3 failures. In particular, it was established that arcing in the tubes occurs when the ion current, which is indicative of the internal gas pressure in the tube, reaches a level of approximately 1×10^{-5} A.

Between January and May 1974, HDL designed and developed an arc protection circuit and initiated an ion-current screening program to evaluate the quality of the vacuum on all vacuum tubes not currently installed in end item devices. In addition, the tube specification was altered to require that the ion current at delivery not exceed 2.5×10^{-8} A and that the change in this current be less than 2×10^{-9} A per month. Five sample A2's were removed from units in the U.S. pipe line to the field and subjected to ion-current screening. One of these tubes was found to be so gassy that it would have arced and destroyed Q_3 upon turn on.

Picatinny Arsenal (PA) was advised of the above actions but exhibited no confidence in screening or other corrective actions without root-cause identification. Picatinny Arsenal advised HDL that a thorough, systematic, organized, and rigorous analysis of the A2 failure to explicitly establish the one root cause was the minimum action considered acceptable.

Consultants from Government and industry participated in this investigation:

U.S. Army Electronics Command (ECOM)
U.S. Army Materials and Mechanics Research Center (AMMRC
Naval Research Laboratory (NRL)
National Bureau of Standards (NBS)
Picatinny Arsenal
Harry Diamond Laboratories
Sandia Corp. (Vacuum Tube Division)

Arthur D. Little Co. (ADL Co.)
General Electric Co. (GE)
The Robert Boyd Co.
Stanley F. Kaisel, consultant

This report summarizes all the root-cause A2 failure-analysis work and analyzes what this work means in terms of the three postulated causes of vacuum degradation in the A2 vacuum bottle.

2. DESCRIPTION OF FAILURE MODES

It has been established that Q_3 failure occurs when gassy A2's arc upon application of voltages. Ion current measurements of defective tubes indicate that tubes whose ion current exceeds 1×10^{-5} A have a high proclivity for arcing. Ion current is proportional to the pressure within the vacuum envelope. Thus, the arcing is attributed to degradation of the ultrahigh vacuum of the tube. The failure analysis team agreed that vacuum degradation is caused by one or more of the following:

Outgassing: degradation of the vacuum by gases emitted from the filament, from the internal surface of the vacuum envelope and electrodes, or from cracks, crevices, or ruptured gas filled cells in the ceramic or braze

Permeation: diffusion of the lighter gases, particularly hydrogen (H_2) and helium (He), through the walls of the system

Leaking: degradation of the vacuum by gas entering the vacuum envelope through cracks or other defects in the material or through the ceramic-to-metal seal interfaces

3. RESULTS OF INVESTIGATIVE TASKS

3.1 Leaking

3.1.1 Flow Rate versus Pore Diameter

Figure 3 plots the flow rate for the air versus the pore radius for a crack length of approximately 10^{-1} cm. This length corresponds to the equivalent leak length characterizing the tube under discussion. This curve indicates that a pore radius of 10^{-6} cm corresponds to a flow rate of 10^{13} Torr liters/s. At this flow rate, a pressure of 10^{-3} Torr in the approximately 0.0005-liter volume of the A2 would be reached in about 1 week. Currently, HDL checks each new tube for gas after a 30-day holding period. This test would easily allow pore leaks of 10^{-6} cm or greater to be detected.

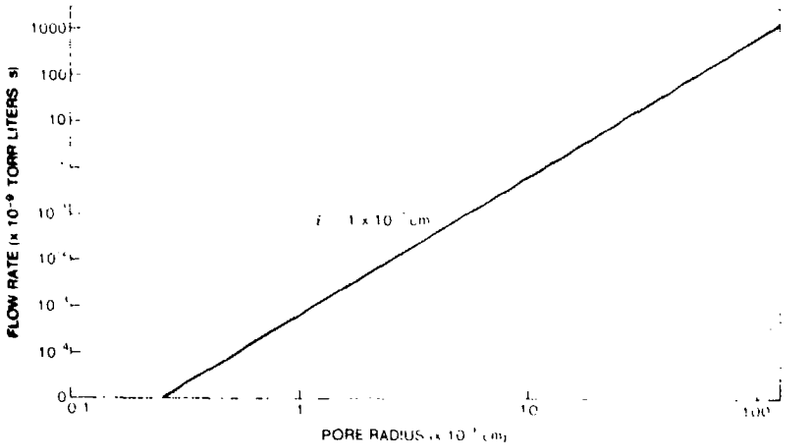

Figure 3. Plot of flow rate for air versus pore radius.

3.1.2 Ceramic Examination

The ceramic from good and bad tubes was examined by scanning electron microscopy (SEM). Even though cracks were observed in all samples, the cracks did not completely penetrate the ceramic body.

3.1.3 Seal Examination

Picatinny Arsenal used SEM with a metallograph and energy dispersive analysis to examine the seals of six sectioned failed A2 assemblies. Leaks were not detected through any seal region. This analysis showed a uniform area of sealing material between each of the junctions.

3.1.4 Seal Characterization

The U.S. Army Electronics Command studied the structure and physical and chemical properties of the metals and alloys used in the seals of good and bad tubes from each vendor. Mictron manufactured the vacuum bottle (fig. 4).

The seal between the niobium (Nb) disk and the copper (Cu) cold-post cathode consists of a Cu-titanium (Ti) alloy and was from 20 to 25 μm thick. The thickness of the alloy was uniform across the entire seal zone, and the boundary against the Nb was extremely smooth. There was no evidence of any Nb in the brazed alloy in good or bad tubes.

The braze between the cold post cathode and its alumina boundary in a bad tube averaged approximately 50 to 54 μm in thickness whereas the braze in a good tube averaged 12 to 25 μm. Each contained Cu, Ti, and silver (Ag). Additionally, the good tube had an Ag-rich region and a $TiCu_3$ phase, while the bad tube had an alloy of Ag and Ti.

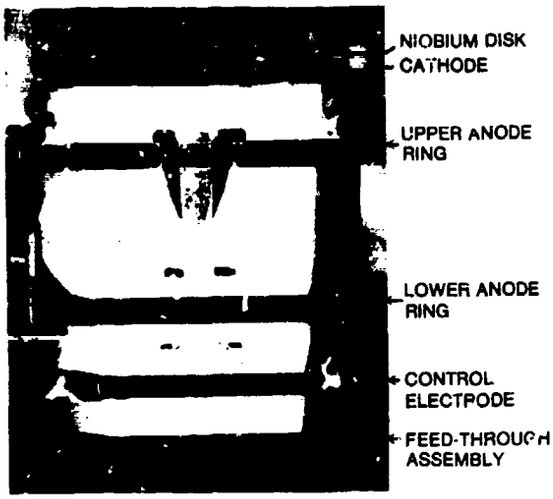

Figure 4. Mictron vacuum bottle, LM-609.

The brazes on the upper and lower sides of the upper and lower anode rings and of the control electrode consisted of a seal joining Cu to the ceramic body. These brazes on both good and bad tubes varied in thickness from 40 to 80 μm. These brazes contained Cu, Ti, nickel (Ni), and gold (Au), whose distributions are illustrated by figure 5. In the filament feed through (fig. 6), the sequence was alumina, molymanganese, and Nb. The braze alloy consisted of Cu, Ni, and Au (NIORO). No significant difference was observed between the brazes of good and bad tubes.

The GE vacuum bottle (fig. 7) is similar to the Mictron vacuum bottle, except that (1) above the cold-post cathode-Nb disk assembly is a Cu cap and (2) a large reentrant is in the alumina immediately above the cold-post cathode and in the third ceramic cylinder immediately below the anode ring.

The brazes of the good and bad GE bottles were examined as were the Mictron bottles. In general, the brazes in the GE bottles were thinner between the Cu and ceramic components than in the Mictron bottles. The difference in thickness of the brazes from fillet to interface and details of the brazes of the Cu cap Nb disk are shown in figure 8. There is also a strong tendency for the braze to build up a large fillet at each end of its parts. Further filleting at all ceramic-Cu corners in good and bad GE bottles is shown in figure 9.

Chemically, the braze in GE bottles consisted of Ti and Cu. Figure 10 shows a probe scan of this braze alloy. Probe microanalysis indicated that this two-phase braze alloy consisted of 22-percent Ti and 78-percent Cu (equivalent to $TiCu_3$), in a matrix of a Cu-rich solid-solution alloy containing 90- to 95-percent Cu and 5- to

10-percent Ti. The $TiCu_3$ phase comprised approximately 50 percent of the fillet area. In these regions, the braze averaged approximately 5 μm in thickness.

The filament feed-through assembly consisted of Cu to molybdenum (Mo) brazed by a Cu-Au solid solution. The Cu-Au braze contained small amounts of Mo.

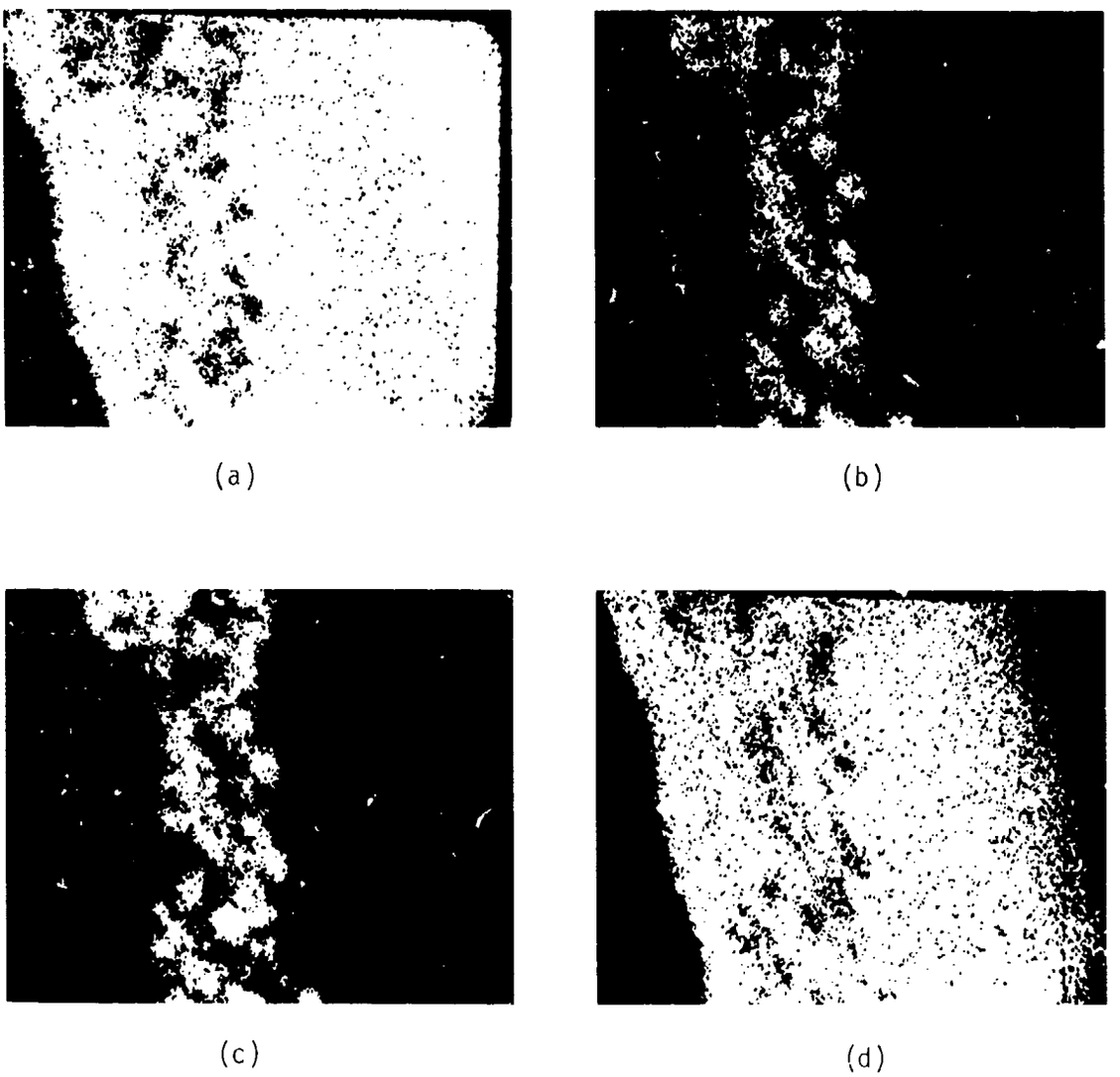

Figure 5. Elements in Mictron tube brazes: (a) copper, (b) titanium, (c) nickel, and (d) gold.

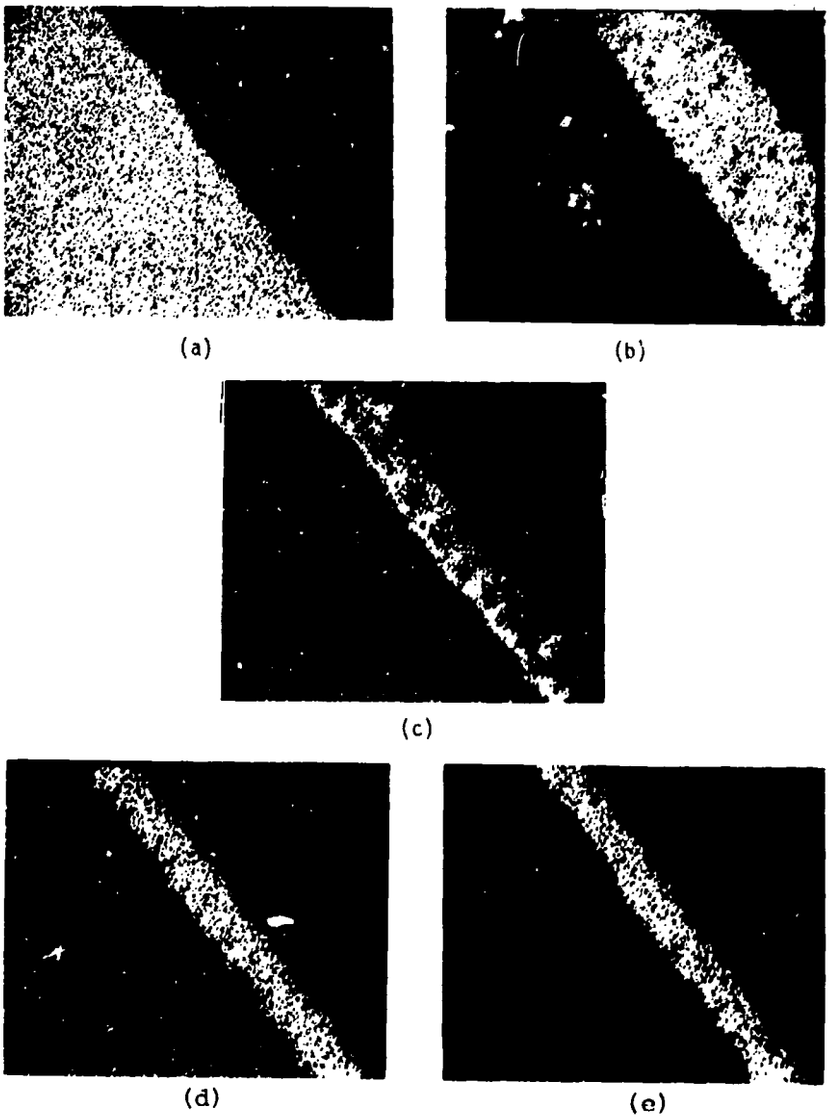

Figure 6. Metallurgy of Micron filament feedthrough: (a) niobium, (b) molymaganese, (c) nickel, (d) gold, and (e) copper.

3.1.5 Gas Analysis

The Naval Research Laboratories opened a defective A2 vacuum bottle in vacuum near a quadrupole gas analyzer. The ambient gases were predominantly nitrogen (N_2) and H_2. The absence of oxygen (O_2), considering that O_2 makes up approximately 5 percent of atmospheric gases, is a strong indication that pore leaks are not present.

Figure 7. General Electric vacuum bottle.

Figure 8. Brazes from fillet to interface and in copper cap niobium disk of General Electric vacuum bottle.

Figure 9. Filleting at ceramic-copper corners in General Electric vacuum bottle.

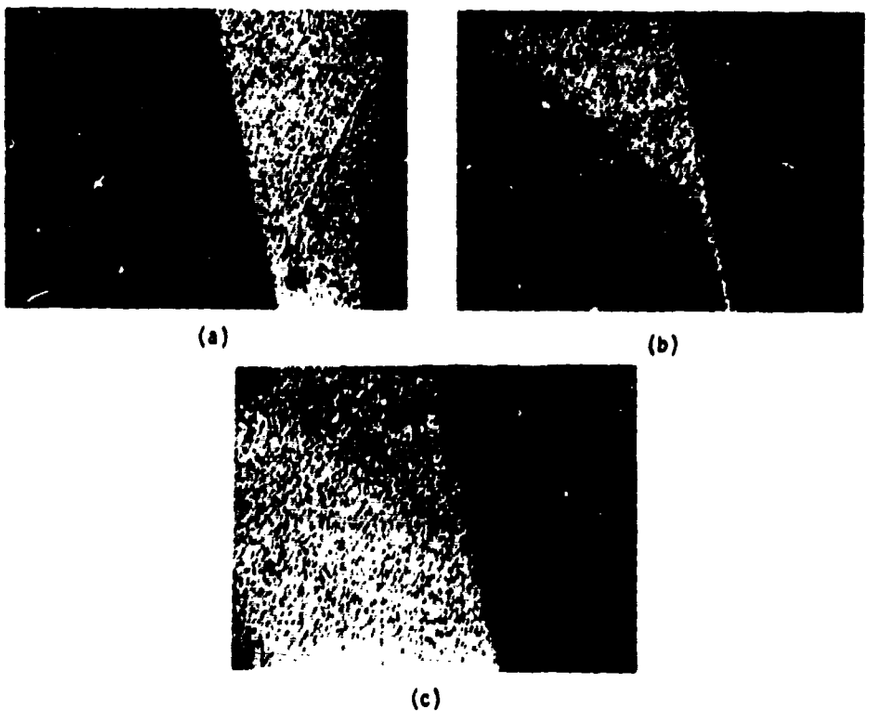

Figure 10. Probe scan of braze alloy in General Electric vacuum bottles: (a) niobium, (b) titanium, and (c) copper.

3.2 Permeation

3.2.1 Permeation Calculations

The Sandia Laboratories calculated the increased H_2 pressure as a function of time and temperature for Nb and Cu using the dimensions in table I. Calculations for the high-alumina ceramic used in the A2 vacuum bottle were not performed since high-alumina ceramics were considered impermeable to gases.

TABLE I. HYDROGEN PRESSURE FOR NIOBIUM AND COPPER

Dimension	Material*		
	Niobium (total)	Copper	
		Each	Total
Area (cm^2)	0.012	0.26 + 0.090 + 0.038	0.3588
Length (cm)	0.072	0.035 + 0.050 + 0.037	0.0807
Area/length (cm)	0.42		9.07

*Internal surface area.

Fick's laws adequately describe the diffusion of gas through solids with a concentration-independent diffusion coefficient, D. That is, the concentration, C, of the diffusing species is given by the solution of Fick's second law:

$$\frac{\partial C(x,t)}{\partial t} = D \frac{\partial^2 C(x,t)}{\partial x^2}$$

which satisfies initial and boundary conditions appropriate to the experiment. Also, the flux of diffusing species at any point in the solid is given by Fick's first law:

$$J = D \text{ grad } C \ .$$

It has been shown* that J can be written as

$$J(x = d,t) = -D\left(\frac{\partial C}{\partial x}\right)_{x=d}$$

$$= \frac{DsPo^n}{d}\left[1 + 2\sum_{n=1}^{\infty}(-1)^n \exp\left(-\frac{Dn^2\pi^2 t}{d^2}\right)\right]$$

where

f(x) = initial distribution of gas in the solid,

d = membrane thickness,

Ds = k (permeation constant),

Po = upstream pressure,

n = ½ (for diatomic gases in metals).

The calculations for Nb used the value of the permeation constant measured by Rudd.[1] The value of the permeation constant was extrapolated to the temperature of interest and is therefore approximate.

The permeation calculation is done for a steady-state condition of motion of H from the outside, into and through the Nb lattice, and into the internal volume. As one can see from table II, for Nb, the diffusion lag time is measured in days, whereas the permeation is measured in hours and minutes.

*Sandia Corp. Report SC-DC-721332, Albuquerque, NM (1964).

[1]R. D. Rudd, J. Phys. Chem., 66 (1962), 351.

TABLE II. EQUILIBRIUM TIMES TO PERMEATE

Material	External pressure (Torr)	Internal pressure at stated time*	
		At 300 K	At 350 K
Niobium	10^{-3}	10^{-3} Torr at 75 days 7 min	10^{-3} Torr at 7 days 2 min
	1	1 Torr at 75 days 4 hr	1 Torr at 7 days 1 hr
Copper	10^{-3}	0.07×10^{-3} Torr at 15.8 yr	10^{-3} Torr at 15.87 yr
	1	5×10^{-3} Torr at 31.5 yr	0.2 Torr at 20 yr

*Number of days = diffusion lag time.

The calculations for Cu used the value of the permeation constant measured by Perkins and Begeal.[2]

The correct interpretation of table II is as follows: If a clean piece of Nb, having the dimensions listed previously, were placed as a barrier between a vacuum, at an atmosphere of 1 Torr of H, and the system held at 300 K, then the vacuum inside would remain for 75 days. Afterwards, the pressure inside would rise to 1 Torr in 4 hr. If the external pressure were 10^{-3} Torr, then the internal pressure would rise to 10^{-3} Torr in 7 min. If the experiment were repeated at a temperature of 350 K, the vacuum would remain for 7 days. Aterwards, the pressure inside would rise to 1 Torr in 1 hr or 10^{-3} Torr in 2 min for external pressures of 1 Torr and 10^{-3} Torr, respectively. However, normal factory processing of Nb usually leaves an oxide coat, which acts as a permeation barrier.

3.2.2 Experimental Studies

3.2.2.1 High-Pressure, High-Temperature Soak

The diffusion-lag-time calculations indicate that high-pressure-soak permeation experiments would be more productive if the temperature were increased and the pressure decreased. Accordingly, the temperature was maintained at 300°C and the pressure held to 1 atm.

Typically, the vacuum envelopes were exposed to a forming gas, comprising 10 percent H_2 and 90 percent N_2 at 300°C and 1 atm for 70 hr. Following this exposure, the envelopes were stabilized by dc operation for the equivalent of 10 ion-current measurement cycles. Next, a standard thermal desorption sequence was run so that a comparison for thermal desorption at temperatures of 200°, 250°, and 300°C could be made for the before and after permeation (table III).

---

[2]*W. G. Perkins and B. R. Begeal, Permeation and Diffusion of Hydrogen in Ceramvar, Copper, and Ceramvar Copper Laminates, Sandia Laboratories Report SC-DC-714493 (1972).*

TABLE III. PERMEATION DATA SUMMARY

Desorption temperature (°C)	Spike ($\times 10^{-9}$ A)		Peak ($\times 10^{-9}$ A)		Residual ($\times 10^{-11}$ A)	
	Before	After	Before	After	Before	After
200	0.28	17	0.38	0.20	0.21	0.15
250	1.9	100	0.48	1.3	0.24	0.15
300	8.0	500	0.70	4.0	0.26	0.21

Thermal desorption data were gathered by a process of cycling the A2 vacuum envelope between room temperature and a sequence of gradually increasing elevated temperatures. At each room temperature portion of the cycle, two ion-current measurements were made.

3.2.2.2 Electrolysis Test

In the electrolytic experiment, it is necessary to form a complete electrolytic circuit consisting of a cathode surface, an anode surface, and an electrolyte. Atomic H is generated electrolytically at the cathode surface, and the H that diffuses through the electrolyte is reionized at the anode surface and detected as an electrolytic current.

The apparatus used for electrolytic testing of the A2's is shown in figure 11. It consisted of an 1800-milliliter flask filled with distilled water to which approximately 30 drops of glacial acetic acid were added. The flask was positioned on a thermostatically controlled hot plate, which maintained the electrolyte just below the boiling point. An anode was formed by coiling platinum (Pt) wire around the thermometer used to measure the electrolyte temperature, while one or more A2 vacuum envelopes (which comprised the cathode of the

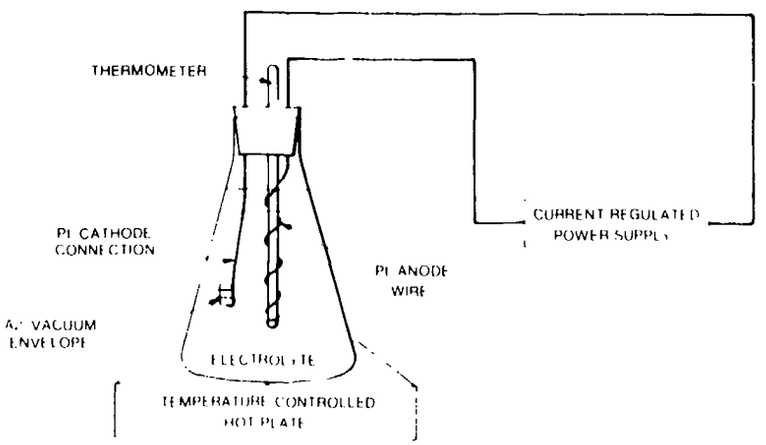

Figure 11. Electrolysis apparatus.

electrolytic cell) were suspended in the electrolyte by a second Pt wire. Connections were made to an external-current-regulated power supply, which was adjusted to pass 10 mA of current through the circuit for every A2 vacuum envelope suspended in the electrolyte.

The seven A2 vacuum bottles (three manufactured by GE, four by Boyd) were subjected to the electrolysis test. After 24 hr, the ion-current trace shown in figure 12(b) was obtained. Figure 12(a) shows the ion-current trace prior to permeation. Figure 12(b) shows that ion current increased several orders of magnitude after electrolysis.

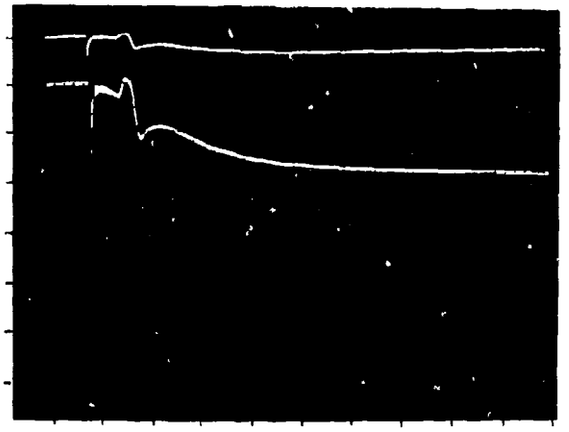

(a)

UPPER TRACE: 10^{-10} A/DIV
LOWER TRACE: 10^{-11} A/DIV
SWEEP: 0.5 s/DIV

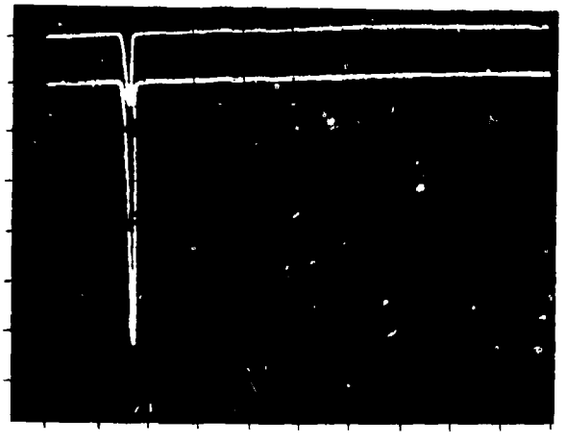

(b)

UPPER TRACE: 10^{-7} A/DIV
LOWER TRACE: 10^{-8} A/DIV
SWEEP: 0.5 s/DIV

Figure 12. Ion-current traces (a) before and (b) after electrolysis (GE 2359).

3.2.2.3 High-Temperature, High-Humidity Test

General Electric investigated improvements needed to increase the storage life of the A2 assembly. During this study several groups of samples were subjected to permeation-enhancing combinations of moisture and temperature. Table IV shows the results of the A2 vacuum-bottle exposure to high temperature, 70°C, and high relative humidity (RH), 95 percent. Generally significant increases in the rate of change of ion current with time were observed after high temperature and high-humidity exposure.

TABLE IV. RATE OF CHANGE OF ION CURRENT ($\times 10^{-B}$/DAY)

Sample	A2 device	Change ($\times 10^{-B}$ A) of ion current/day in various environments						
		Helium						70°C 95% RH
		2	5	1	2	3	3	1
A	1045	69	12	40	70*	33	25	1000+
	5696	0.4	0.4	1.2	2*	0.7	0.3	1000+
	5730	4.0	0.4	1.0	109*	No test	No test	300+
	5704	0.5	0.6	1.3	2*	0.7	1	3
		Shelf						70°C 95% RH
		2	6	5	7	1		3
B	1747	--	0	--	0	0*		0
	*1	--	0.9	--	0.12	0.03*		0.33
	2174	0.25	--	0.32	-	3.6*		1000+
	6121	0.25	--	1.0	--	4.5*		100+
		Shelf			<0°C 95% RH			70°C 25% RH / 95% RH / 95% RH
		1	1	5	1	2	1	3 / 2 / 5
C	2030	0*	0	0	0	0	0	0 / 2 / 250
	1868	1.7*	1.3	0.3	0.7	0.5	0.5	1.4 / 1.2 / 6
	2153	0.05*	0.1	0.07	0.05	0.5	0.05	0.6 / 0.5+ / 6
	6111	3.2	2.2*	3.4	2.0	3.3	2.5	9 / 20 / 1000+
		Hydrogen				Shelf			70°C 95% RH
		2	5	1	1	1	4	3	3
D	1994	0	0	0	0*	0	0	0	100+
	*2	1.25	0	0	--*	--	--	--	--
	1971	1	1	1.2	0.6*	1.3	0.5	1.0	30
	1870	0.16	0.16	0.18	1.1*	0.1	0.1	0.15	1000+

*Potting removed.
--No data taken.

Recently, the ADL Co. conducted high-temperature, high-RH permeation-enhancing tests and used these results to calculate the mean time to failure for storage temperature of 100°C and an RH of 100 percent.

Specifically, A2 vacuum bottles from GE and Boyd were checked for ion current after thermal desorption was conducted at 100°, 200°, and 300°C before and after permeation-enhancing high-temperature, high-humidity tests. Then HDL used these data with flow-rate permeation equation (1) to calculate the time required to reach catastrophic gas levels (10^{-4} Torr), assuming that permeation is the only gas buildup phenomenon occurring and that pumping or cleanup action is not taking place:

$$Q = \alpha \Delta P^{n} e^{-B/T} , \qquad (1)$$

where

Q = gas flow rate (Torr liters/second),

ΔP = change in pressure (Torr) occurring over the temperature range t,

T = temperature (degrees Kelvin),

n = ½ (used since the gas exists as diatomic molecules outside the permeation barrier, but after dissociation diffuses as free atoms through the solid; such is the case in the electrolysis experiment),

α,B = constants depending upon A2 physical characteristics.

A plot of permeation flow rate versus temperature at 1 atm of water vapor for two GE units is shown in figure 13. This plot shows a -lnQ value of 22.5 and 23.6 for the two GE units at 70°C. From these data, a straightforward calculation shows that if the tubes are stored at a temperature of 70°C and an RH of 100 percent, the time t (years) required to reach a pressure of 10^{-4} Torr is $33.4 \leq t \leq 100.4$.

This calculation shows that the observed vacuum degradation was not caused by permeation, since storage conditions are less severe than

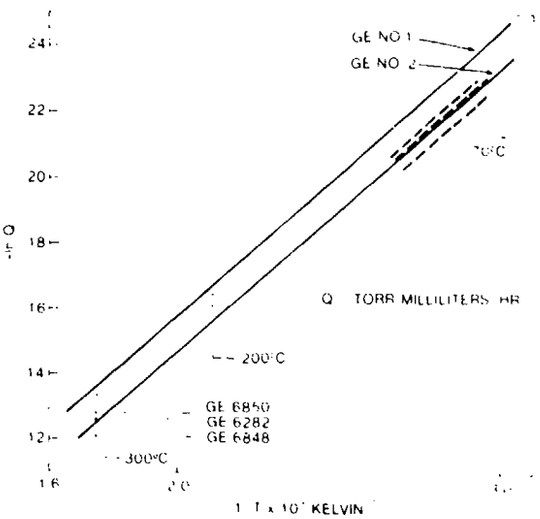

Figure 13. Permeation rate versus temperature at 1 atm of water vapor.

those of the calculations. Boyd-manufactured vacuum bottles exhibit no permeation susceptibility, and thus no graphs for these bottles were plotted.

3.3 Outgassing

Vacuum-tube manufacturers are aware that contamination on the surface of tube parts can act as sources of gas. Because of this action, much time and attention are paid to the problem of using the cleanest possible parts in the vacuum-tube construction. After the most meticulous cleaning process is completed, gases still evolve from the material if sufficient heat is applied. When the final vacuum-tube seal is made, invariably, some of this gas is adsorbed on the tube surfaces and can be desorbed under certain conditions of temperature and pressure. The average time, t_{av}, that an adsorbed particle spends on a surface can be calculated from

$$t_{av} = \lambda_o e^{E_D/RT} ,$$

where

λ_o = period of oscillation of the molecule normal to the surface ($\lambda_o = 10^{-13}$ s),

E_D = activation energy for desorption

R = universal gas constant,

T = temperature absolute.

Thus, weakly bound atoms or molecules desorb at different times, depending on the surface temperature and the activation energy for desorption.

3.3.1 Thermal Desorption

The failure analysis team suggested that thermal desorption tests would provide a measure of what the ion-current turn-on phenomenon might be after long-term storage. This phenomenon will be due to the outgassing of residual gases initially trapped in the tube. Many desorption tests at different temperatures have been conducted and evaluated. It is the consensus of the failure analysis team that desorption at 300°C for a minimum time of 1 hr is required to establish the long-term equilibrium turn-on behavior of the A2 vacuum bottle, due to the outgassing of initially trapped residual gases.

Thermal desorption tests on newly processed vacuum bottles manufactured by GE and Boyd were conducted at 150°C. Later, Boyd manufactured vacuum bottles that were thermally desorbed at 300°C. The results of these thermal desorption tests are shown in table V.

TABLE V. THERMAL DESORPTION TESTS

Manufacturer	Desorption temperature (°C)	Ion current (I_D)	
		I_D av ($\times 10^{-8}$)	I_D range ($\times 10^{-8}$)
General Electric	150	0.5	0 to 10
Boyd	150	4.7	4 to 99
Boyd	300	4.2	2 to 120

3.3.2. Quadrupole Gas Analysis

Using the quadrupole mass analysis technique, NRL determined the magnitude and type of gas released from thermal and electron desorption. Desorption experiments were conducted on A2 vacuum bottles removed from A2 assemblies. Some of these assemblies had failed the HDL ion-current specification; others had passed. These A2 vacuum bottles were drilled in vacuum and positioned so that the gases released on breakthrough would pass near the quadrupole for analysis. After the hole had been drilled, the gases in the A2 vacuum bottle were observed when the filaments were heated (thermal desorption) and when voltages were applied to the electrodes (electron desorption). It was determined from this experiment that the types of gas released from desorption were chiefly of mass 28 (N_2) and mass 2 (H_2). Also, some increases in hydrocarbons of masses 14, 15, and 16 were observed. Similar gases were observed in the vacuum space prior to desorption experiments.

The increase in pressure in the approximately 0.0005-liter volume of the A2 vacuum envelopes of good tubes averaged 5×10^{-4} Torr for thermal desorption, whereas it averaged 1.6×10^{-2} Torr for bad and marginal vacuum bottles. The specific data on thermal desorption and electron desorption for each tube are shown in table VI (page 25).

3.3.3 Thermal Desorption on Temperature Cycles A2 Envelope and Cavity Subassemblies

Picatinny Arsenal removed 12 vacuum bottles and cavities from their A2 assemblies and subjected them to thermal shock testing. The shock sequence consisted of alternate immersion of the units into a temperature bath of isopropyl alcohol at -50°C and water at 100°C for a

TABLE VI. THERMAL AND ELECTRON DESORPTION IN VACUUM TUBES

A2 device	Gas in tube before desorption (type, pressure)	Gas type and pressure observed from	
		Thermal desorption	Electron desorption
1252 very good	--	5×10^{-4} (N_2)	6.6×10^{-5} (N_2)
5635 marginal	2.5×10^{-4} (H_2, CO_2)	1.4×10^{-2} (H_2, He, C, N_2)	1.5×10^{-2} (CH_3, CH_4, N_2)
1478 bad	3×10^{-3} (N_2)	1.1×10^{-2} (N_2)	2.4×10^{-3} (N_2)
1552 very bad	5×10^{-3} (N_2)	2.3×10^{-2} (N_2)	2.6×10^{-3} (N_2)

3-min minimum immersion time. The time between immersions was less than 5 s. Some of these devices exhibited large increases in ion current after a few cycles, and by the end of 60 cycles, all of the devices increased more than one order of magnitude in ion current.

Five of these A2 vacuum envelopes and cavities were sent to the ADL Co. for thermal desorption tests at 300°C to assist in determining the cause of the induced gas buildup. Preliminary desorption at 300°C indicated that the ion currents would be at a high enough level to saturate the ion-current tester. Accordingly, the thermal desorption was conducted at 100°C on four GE assemblies (table VII).

TABLE VII. ION CURRENT READINGS FOLLOWING 100°C THERMAL DESORPTION

A2 device	Spike (A)	Peak (A)	Residual (A)
1481	(*)	(*)	2.2×10^{-6}
5495	1.4×10^{-6}	5.4×10^{-6}	5.2×10^{-7}
5571	(†)	1×10^{-4}	1×10^{-4}
1620	5.5×10^{-8}	5.6×10^{-8}	7×10^{-9}

*Spike and peak buried in off-scale response >1 × 10^{-4}.
†Spike not discernible.

3.4 Ceramic Microcracking

Because of the design and construction of the A2 vacuum envelope, significant stresses are developed in the ceramic when the device cools from the high temperature at which the tube was sealed. These stresses are relieved in part by plastic deformation of the Cu parts, while still in the annealing temperature range, and in part by formation of microcracks in the ceramic material.

At NRL, a possible virtual leak mechanism was postulated. This was caused by cracks propagating out from the inside wall and connecting and erupting gas-filled pores within the ceramic to the interior of the A2 vacuum envelope. To explore this postulate, the failure-analysis team propo· ad the following experiments:

a. Calculate the residual stresses developed in the vacuum envelope due to the assembly brazing operating.

b. Characterize the ceramic from good and bad vacuum bottles.

c. Fracture ceramic parts in the presence of a quadrupole gas analyzer to determine the type and magnitude of the gas released.

d. Conduct stress tests on sample ceramic pieces.

e. Perform acoustic emission measurements to determine if thermal expansion mismatch is causing crack spread in the tube walls.

f. Conduct temperature shock tests to determine if microcrack spread can be accelerated (size and number of pores cut by microcrack length).

The results of the first five experiments are as follows:

3.4.1 Residual Stress Calculations

Sandia Laboratories used the finite element computer code SASL to analyze the residual stresses developed in the vacuum tube (fig. 14) due to the brazing operation. Calculations were made for stress-free temperatures (Ti) of 870°, 600°, and 400°C.

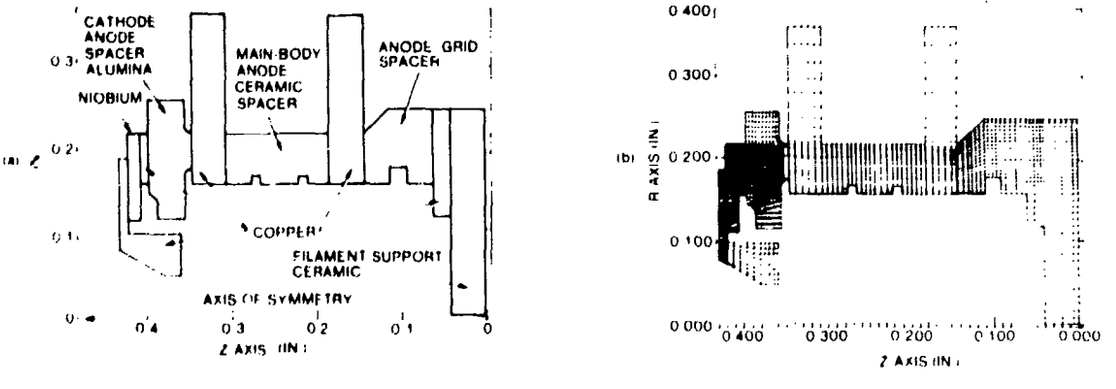

Figure 14. Residual stress: (a) vacuum tube and (b) finite-element idealization.

The calculated contours of maximum principal stress in the R-Z plane in the ceramic for the assumed stress-free temperature of Ti = 870°C are shown in figures 15 to 18. Figure 15 shows the calculated stress contours:

A = 28,809 psi--84,307 kg/cm^2
B = 17,600 psi--51,505 kg/cm^2

in the anode cathode spacer. Figure 16 shows four areas of high stresses:

C = 20,618 psi--60,337 kg/cm^2
D = 15,657 psi--45,819 kg/cm^2
E = 20,849 psi--61,013 kg/cm^2
F = 14,805 psi--43,326 kg/cm^2

in the main body. Figure 17 shows two areas of high stresses:

G = 20,703 psi--60,586 kg/cm^2
H = 14,306 psi--14,865 kg/cm^2

in the anode grid spacer. Figure 18 shows one area of high stress in the filament support ceramic. The maximum principal stress is:

I = 12,073 psi--35,330 kg/cm^2.

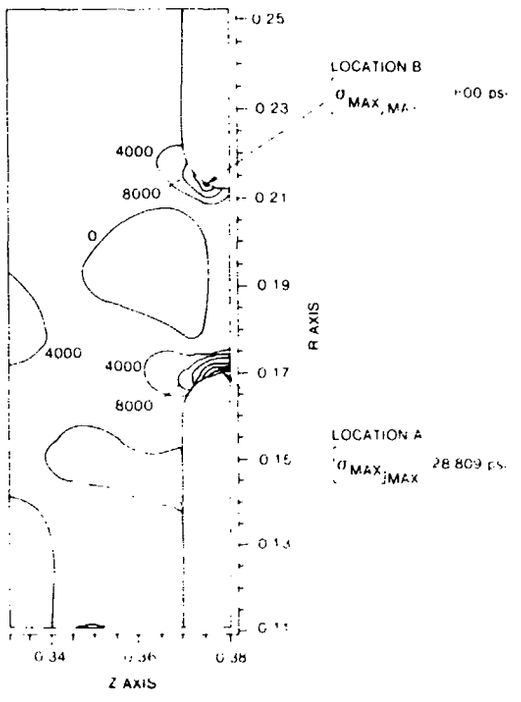

Figure 15. Maximum principal stress in R-Z plane contours in anode/cathode spacer, T_i = 870°C.

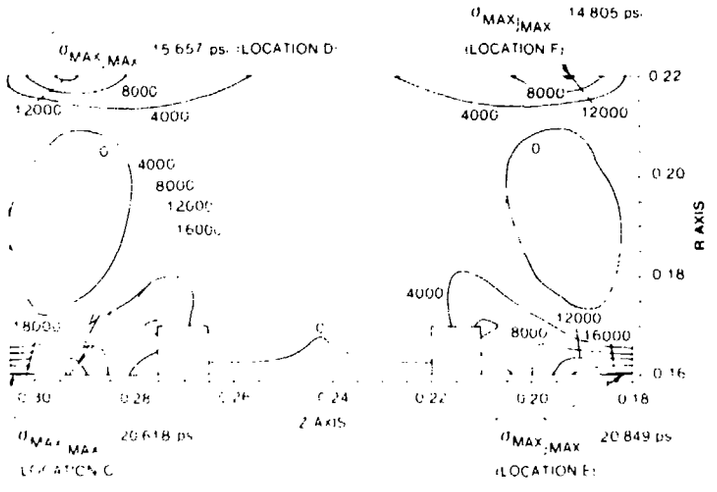

Figure 16. Maximum principal stress in R-Z plane contours in main-body anode ceramic spacer, T_i = 870°C.

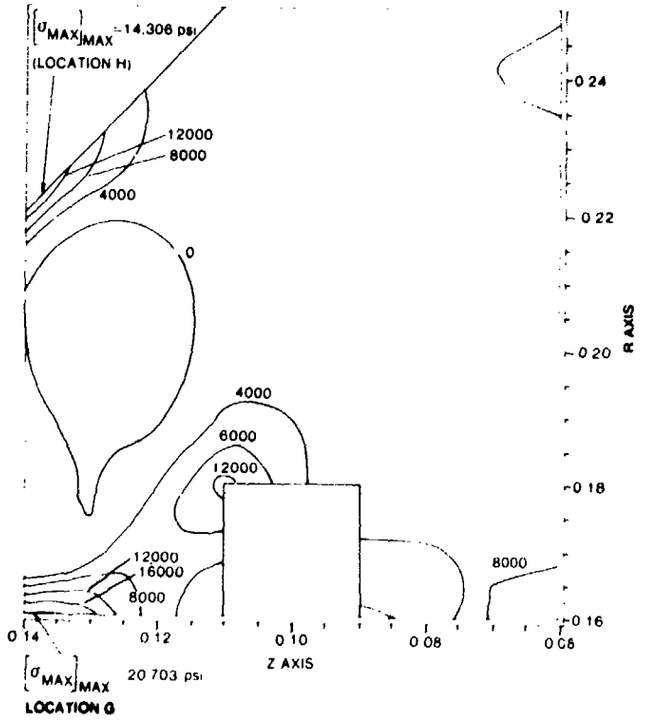

Figure 17. Maximum principal stress in R-Z plane contours in anode/grid spacer, T_i = 870°C.

Figure 18. Maximum principal stress in R-Z plane contours in filament support ceramic, T_i = 870°C.

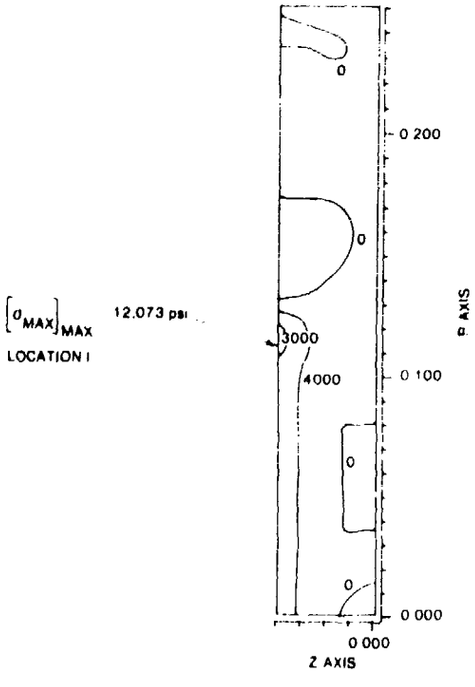

When the assumed stress-free temperature of the structure is lowered, the maximum stresses developed in the ceramic also are lowered. Table VIII shows the peak maximum principal stresses in the R-Z plane at the designated locations.

TABLE VIII. MAXIMUM PRINCIPAL STRESS IN R-Z PLANE AT DESIGNATED LOCATIONS

Component	Location	Stress (psi) at stress-free temperature		
		At 870°C	At 600°C	At 400°C
Anode/cathode spacer	A	28,809	18,925	15,258
	B	17,600	19,242	14,707
Main-body anode spacer	C	20,618	17,176	13,226
	D	15,657	13,744	10,616
	E	20,849	17,788	13,865
	F	14,805	12,364	9,452
Anode/grid spacer	G	20,703	17,593	13,741
	H	14,106	12,248	9,690
Filament support ceramic	I	12,073	9,903	7,267

This analysis shows that the anode/cathode spacer is the highest stressed ceramic in the tube. At a stress-free temperature of Ti = 870°C, the maximum stress is essentially the same as the failure strength of the alumina. For a stress-free temperature of Ti = 600°C, the maximum calculated stress is approximately 70 percent of the tabulated failure strength of the ceramic and for the stress-free temperature of Ti = 400°C, the maximum calculated stress is approximately 50 percent of the tabulated failure strength of the alumina.

3.4.2 Ceramic Characterization

At AMMRC, hardness studies were conducted on polished sections of ceramics used in the A2 vacuum envelope. Density measurement of this ceramic also was made, and the apparent porosity was calculated from the difference between measured and theoretical densities. Table IX shows the measured density, percentage of Al_2O_3, theoretical density, and apparent porosity for the ceramic sample from A2 vacuum bottles manufactured by GE, Boyd, and Mictron. Knoop hardness values were determined as a function of distance from the braze interface and compared with hardness values of similar ceramic pieces not yet used in vacuum-tube construction. The results indicated that the hardness of the new ceramic remained constant. But the hardness of the ceramic in the tubes decreases markedly as the braze interface is approached.

TABLE IX. DENSITIES OF CERAMIC USE IN VACUUM-BOTTLE CONSTRUCTION

Tube vendor	Al_2O_3 (wt %)	Measured density (g/cm^3)	Theoretical density (g/cm^3)	Apparent density (vol. %)
General Electric	97	3.76 3.76 3.77 3.78	3.87	2.84 2.84 2.58 2.33
Boyd	97.6	3.76 3.79	3.89	3.34 2.57
Mictron	96 to 97.6	3.75 3.90	3.87 to 3.89	3.1 to 3.6 1.31 to 2.31

Density measurements and SEM studies indicated the presence of pores. The observed pores are basically in a bimodal distribution. The larger population of pores consists of small pores about 5 μm in size and often spaced about 20 μm apart. The remaining population consists of larger pores about 20 μm in size and often spaced 40 μm apart.

3.4.3 Ceramic Fracture in Vacuum

At NRL, an ultrahigh vacuum system for a minimum volume of 2 liters was designed to monitor the gases liberated when ceramic samples were crushed near a quadrupole gas analyzer. The system features an externally controlled stress device on the ceramic sample and records the atomic masses of the gas released with each acoustic crack event. It could also monitor these optimally, so the cracks could be counted. Samples from six tubes were crushed by this system. The results of these tests are shown in table X.

TABLE X. NITROGEN BURST OF TRAPPED GAS IN CERAMIC VOID

Ceramic	Total pressure per crack (Torr)	Cracks (No.)	Pore size (3% porosity) (μm)
General Electric			
GE-3	[illegible]	4	4.7
GE-4	1.1×10^{-7}	4	6.3
GE-5	1.1×10^{-7}	6	6.3
Mictron			
VT-1	1.4×10^{-7}	7	7.4
VT-2	[illegible]	[illegible]	[illegible]
VT-3	[illegible]	[illegible]	[illegible]

These data indicate that the average pore size in the ceramic is approximately 6.3 μm. It also shows that the predominant gas in the ceramic is N_2 and that the average increase in pressure per crack is 10^{-2} Torr. The pore size along the fractures is determined from measuring escaping gases ranging from 3 to 20 μm. Figure 19 shows the increase in N_2 burst of trapped gas in ceramic voids as a function of fracture propagation.

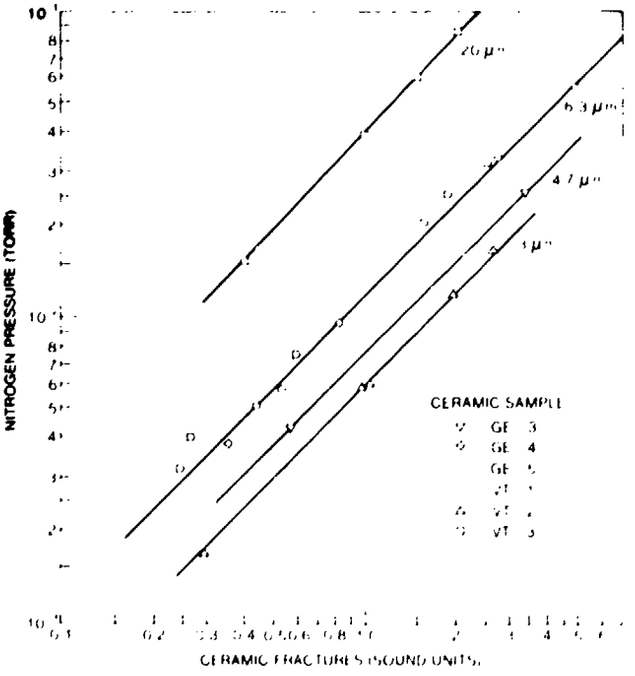

Figure 19. Nitrogen burst of trapped gas in ceramic voids.

3.4.4 Stress Test on Ceramic Pieces

Also, NRL determined the tensile strength of the ceramic used in the vacuum bottles. A tensile failure stress system was constructed, which consisted of machining and epoxying brass grips on the ends of seven bottles. A flexible linkage system and spherical loading seats were used to minimize any parasitic torsion or bending loads. Such tests were attempted on six components. Two components failed; the other four had epoxied brass grips break off at stresses of 1500 to 10,000 psi (4390 to 29,264 kg/cm^2). Another sample failed at approximately 15,000 psi (43,896 kg/cm^2) after the brass grips were rebonded to it. All three failures occurred exclusively in the ceramic (Al_2O_3), with the fracture only occasionally approaching the seal material.

3.4.5 Observations of Microcracks

At AMMRC, cracks were observed in the ceramic; the cracks started at the corner adjacent to the Cu and propagated into it. Some cracks ended at a free surface close to their point of origin; others continued into the ceramic. Some tubes that fractured during handling showed crack paths that originated with these corner cracks. All tubes examined had corner cracks. From 34 to 83 percent of the corners of any one tube showed the cracks.

According to ECOM, fracturing is common in the ceramics of all vacuum bottles examined. Such cracking typically develops at the outer and inner corners of the ceramic and near the braze at the corners. The cracks may end in the ceramic body or arcuately begin and end near the braze contact. When similar cracks resulted in the catastrophic failure of two GE bottles during preliminary sample preparation, the cold-post cathode assembly separated from the rest of the sample. Photomicrographs show typical microcracks in the ceramic near the seal interface (fig. 20).

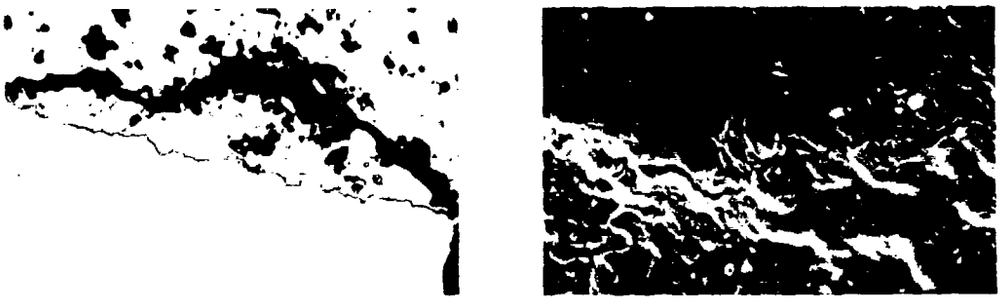

Figure 20. Typical microcracks in ceramic near seal interface.

The ADL Co. reported that during the first thermal desorption run of two GE vacuum bottles, the vacuum envelopes went to air at the first 200°C thermal cycle. A dye check on these samples showed four very faint cracks in the cold cathode end ceramic. At NRL, some sample A2 bottles cracked near the cold-cathode ceramic interface, and one bottle cracked at the filament end during immersion in solvents. Sandia, PA, and HDL also observed cracking in the ceramic of some samples during test preparation.

3.4.5.1 Acoustic Emissions

The overwhelming evidence that vacuum bottles crack prompted the failure analysis team to seek correlation between cracking and gas increases. It is well known that cracking ceramic is accompanied by acoustic emission. Thus, an experiment was proposed to detect acoustic emissions and see if emissions could be correlated with release of gas from pores in the ceramic by propagating microcracks. An acoustic emission task was assigned to NBS and to the ADL Co. At NBS, acoustic emission was measured on six A2 vacuum bottles of known ion current. The bottles were cooled in an alcohol-water mixture to -30°C. Cooling occurred over a 7-min interval to avoid temperature shock stresses. A Dunnegan transducer with a 160-kHz resonant frequency was used to detect the acoustic emissions. The

transducer was acoustically coupled to the alcohol-water mixture with a brass rod. Acoustic emissions were stored on an NBS-constructed monitor and then fed into an electronic computer for analysis.

Acoustic emissions occurred on all tubes as they were cooled to -30°C. However, ion-current tests conducted after the conclusion of the acoustic emission tests could not be correlated with the emissions. The ion current before and after the acoustic emission tests is shown in table XI.

TABLE XI. ACOUSTIC EMISSION TESTS AND ION CURRENT

A2 device	Acoustic emissions		Ion current ($\times 10^{-8}$) (A)	
	Run No. 1	Run No. 2	Before	After
924	37	0	1,600	880
936	30	4	16,000	16,000
934	23	1	1,600	3,000
929	28	14	12	64
909	37	16	42,000	Air

The ADL Co. measured acoustic emissions on eight A2 vacuum bottles. Each bottle was cycled from the ambient temperature to the cold bath (0°C, 2 min) to the hot bath (45°, 100°, or 120°C, 2 min) and back to ambient (in air until cooled to 25°C). While the bottle was in the hot bath, acoustic emissions were detected by a ceramic piezoelectric transducer cemented to a glass beaker. Depolarization was precluded by bonding a low-conductivity glass rod between the transducer and the beaker. Another rod 1/4 wavelength long was cemented to the other surface of the piezoelectric disk to maximize the acoustic coupling at the operating frequency of 37 kHz. Figure 21 shows the setup of the hot bath with the transducer. The acoustic emission data after amplification and filtering were displayed on the face of a memory cathode-ray-tube (CRT) oscilloscope. All vacuum tubes produced acoustic emissions to varying degrees as shown in table XII. Each tube was cycled 50 times between 0° and 120°C, and the ion currents were recorded every fifth cycle. The results of these tests are shown in figures 22 to 24.

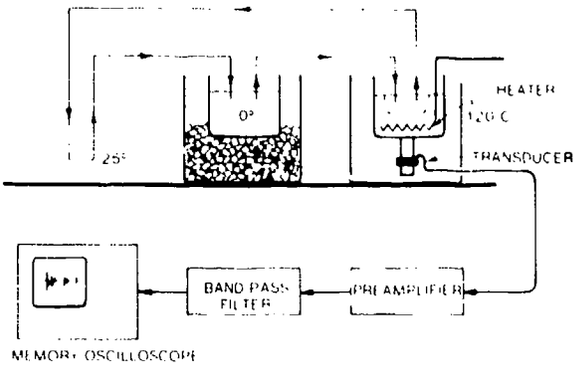

Figure 21. Apparatus for receiving and recording acoustic emissions during heat stress cycle.

TABLE XII. ACOUSTIC EVENTS PER CYCLE FOR VACUUM TUBES

Manufacturer	A2 device	Acoustic events/ cycle
General Electric	2358	4.7
	2359	2.0
	6303	1.7
	6306	4.1
Boyd	937	2.8
	939	2.2
Mictron	7455	2.7

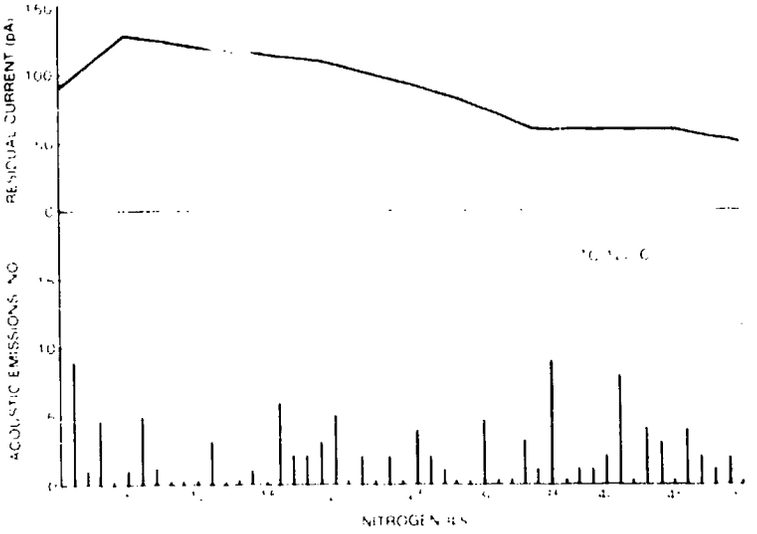

Figure 22. Acoustic emission of vacuum tube (GE 2359).

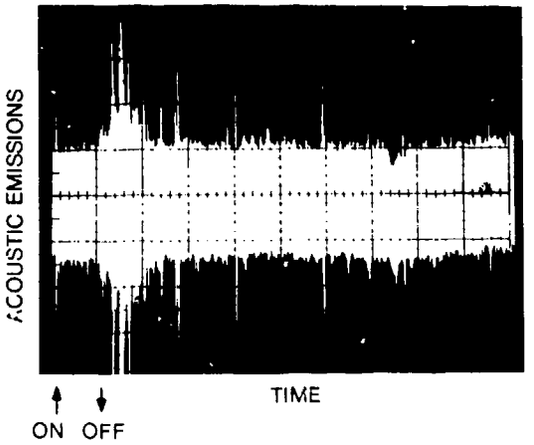

Figure 23. Acoustic emissions associated with thermal shock produced by filament cycling (device GE 2358 at 25°C).

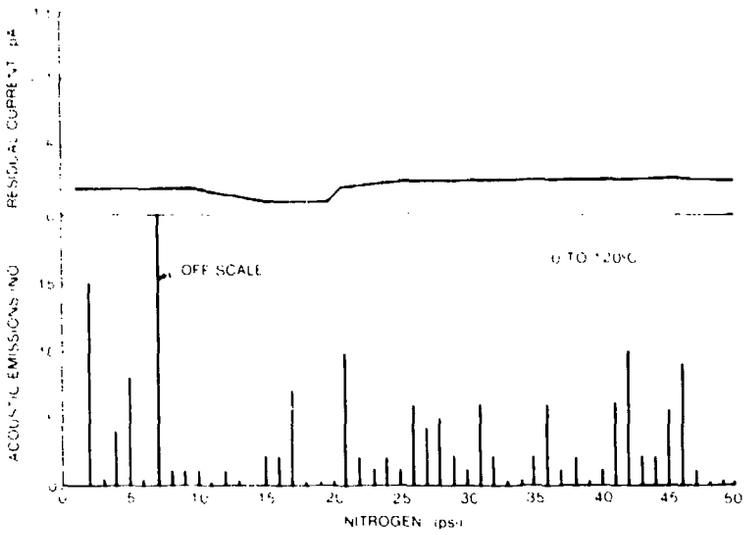

Figure 24. Acoustic emission of vacuum tube (GE 6306).

Recently, HDL performed additional acoustic emission studies at slowly varying and constant temperatures and with newly developed instrumentation, which permitted simultaneous acoustic-emission and ion-current measurement.

Six A2 vacuum envelopes and six A2 vacuum envelope/cavity assemblies were maintained at -35°C for 3 hr while acoustic-emission and ion-current data were monitored. For these tests, many gas bursts occurred, but few acoustic emissions were observed. It is believed that acoustic-emission observation may have been hampered by the limited frequency response of the chart recorder.

3.4.5.2 Size and Number of Pores Cut by Microcrack Lengths

At ECOM, 17 vacuum bottles and cavities (7 manufactured by GE and 10 by Boyd) were cut in half, potted, and examined by light microscopy, SEM, and electron microprobe. These are results of these observations:

a. General Electric vacuum bottles

(1) Twenty-three percent of all potential internal crack sites showed cracks with a total average crack length per GE bottle of 0.74 mm intersecting 10 pores, 20 μm in diameter and 9 pores, 10 μm in diameter. These correspond to a pressure rise of 7.2×10^{-6} Torr and 6.3×10^{-6} Torr, respectively.

(2) Fifty-four percent of all braze-ceramic interfaces inside bottles were cracked.

(3) From crack area measurements, approximately 540 pores, 20 μm in diameter, and 1026 pores, 5 μm in diameter, would be cut by cracks.

Interruption at 540 pores, 20 μm in diameter, would cause a pressure rise of 3.4×10^{-3} Torr; interruption at 1026 pores, 5 μm in diameter, would cause a pressure rise of 10^{-4} Torr. Thus, the total pressure rise in the GE tubes would be 3.5×10^{-3} Torr.

b. Boyd Vacuum Bottles

(1) Eighty percent of all Boyd bottles checked had cracks at internal bottle surfaces.

(2) Twenty-four percent of all potential crack sites showed cracks with a total average crack length per bottle of 0.74 mm intersecting approximately 15 pores, 10 μm in diameter, corresponding to a pressure rise of 1.2×10^{-5} Torr.

(3) From crack area measurements, approximately 225 pores, 10 μm in diameter, would be cut by cracks. The pressure rise corresponding to cutting 225 pores, 10 μm in diameter would be 2.6×10^{-5} Torr or an ion current reading of $2.65/1.5 \times 10^{-7}$ A.

4. OTHER WORK

4.1 Calibration of HDL Ion-Current Tester

Early in the failure-analysis effort, HDL recognized the need for a vacuum-tube gas tester that could be used by tube vendors and others to determine the quality of the vacuum in tubes proposed for government use. Therefore, HDL designed a tester that could measure vacuum degradation in terms of ion current. The tester works on the principle that electrons emitted by the filaments and accelerated by the positively charged control ring produce ions upon colliding with gas molecules. These positively charged ions are attracted to the negatively charged anode and counted by the current meter in series with the anode (fig. 25).

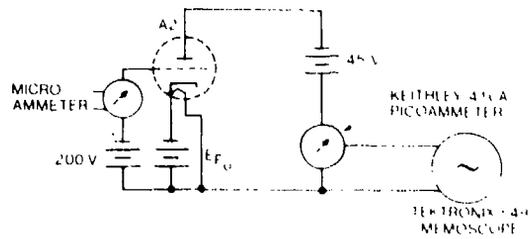

Figure 25. Ion-current tester.

Then for a given number of electrons available, the number of ions thus created depends on the number of gas molecules present and on the pressure in the tube. It is, therefore, possible to determine relative pressure by measuring ion current. Hence, HDL used this current as an acceptance criterion for purchasing A2 assemblies. Later, NRL and HDL established that ion current and pressure are related as follows:

$$\text{Pressure (Torr)} \simeq 150 \text{ ion current (A)} .$$

4.2 Work by General Electric

General Electric studied vacuum bottles, to propose a program that will culminate in A2 assemblies having a storage life of at least 20 yr.[3] The following is a summary of these investigations.

The A2 pressure change is substantially linear in most bottles, although the rate of change may vary from tube to tube. This characteristic is indicative of permeation, rather than release of gas by microcracking of the ceramic or by release of gas due to desorption of gas that was not adequately pumped out.

Therefore, GE tested five groups of samples to determine the effects of permeation-enhancing combinations of moisture and temperature. Ten A2 bottles represented a range of gas-pressure variation from 0 to 4.5×10^{-8} A per day. The samples were listed in ascending order of their rate of ion-current increase, and then every fourth sample was placed in group A, B, C, or D, giving four groups with a range of ion currents from low to high in each group. Subsequently, a fifth group, E, of three bottles was added for more data. The groups were exposed to the sequence of environments listed in table XIII.

TABLE XIII. TESTING OF ION CURRENT

Group	Environment sequence						
	Step 1	Step 2	Step 3	Step 4	Step 5	Step 6	Step 7
A	Shelf	Humidity	Shelf	Vacuum	Shelf	100°C	Shelf
B	Shelf	100°C	Shelf	Humidity	Shelf	Vacuum	Shelf
C	Shelf	Vacuum	Shelf	100°C	Shelf	Humidity	Shelf
D (control)	Shelf	Shelf	Shelf	Shelf	Shelf	Shelf	Shelf
E	Shelf	Shelf	Shelf	140#N2	Shelf	Vacuum	Shelf

[3] *Investigations to Determine Improvements Needed to Increase Storage Life of A2 Assemblies, General Electric Co., Schenectady, NY (14 February 1975).*

As a result of these exposures, the most severe ion-current increases occured when the A2 assemblies were exposed to high temperature (75°C) and high humidity (95 percent) simultaneously. The gas buildup phenomenon was concluded to be caused by permeation, and, therefore, Nb should not be used as a portion of the vacuum envelope. Specifically, GE proposed the following programs:

a. Redesign the basic vacuum structure to reduce stresses in ceramic use, higher kiloinches per second (KIPS) ceramic (40 KIPS versus 28 KIPS).

b. Eliminate the use of Nb from vacuum envelopes.

c. Investigate the use of molymanganese metallized ceramic seal surfaces and changes to braze washers.

d. Improve the brazing schedule.

e. Produce twenty-five 1A2 and twenty-five 2A2's for evaluation.

However, HDL rejected the GE proposal and instead awarded GE a contract for fabricating and testing sample A2 vacuum bottles, incorporating recommendations made by the failure-analysis team.

The objectives of this second contract were to construct sample vacuum envelopes using molymanganese metallized ceramic seal faces and eliminate Nb, Ag in the braze material, Ti, or Ta in the seals. If Nb is desired for gettering, it must be used in such a way that it will not provide a path for permeation.

General Electric evaluated three designs before deciding on the final design to be used in the first article sample evaluation:

Group 1 was made with molymanganese metallized ceramic seal faces and NIORO-plated Nb cathode washers, each concentric with an inner unplated Nb washer.

Group 2 was made with molymanganese metallized ceramic seal faces, NIORO brazing washers, and Cu-plated Nb cathode washers, undercut to remove the Cu from the surface exposed to the vacuum.

Group 3 was made with molymanganese metallized ceramic seal faces, a Mo cathode support washer, a NIORO brazing washer, and a Ti gettering rod in the exhaust hole of the hollow cold-post cathode.

Each group of vacuum bottles was subjected to a series of 10 tests:

Test No. 1.--Gas after exhaust: The groups showed no significant differences (they differed less than one order of magnitude), and none met the specifications of 10^{-6} A.

Test No. 2.--Direct current for 12 hr and then measurement of gas: All groups showed no ion current on a scale of 1×10^{-8} A.

Test No. 3.--Five cycles of immersion in boiling water and ice water and then measurement of gas: The groups showed no significant differences, and they all met the specifications.

Test No. 4.--Electrolysis for 24 hr: Group 3 samples had significantly lower ion current after electrolysis, although each group had one sample appreciably higher than the others in the group.

Test No. 5.--Heat to 300°C for 1 hr and then measurement of gas: Group 3 samples had significantly lower ion current after heat, although each group had one sample appreciably higher than the others in the group.

Test No. 6.--Humidity test for 3 days and then measurement of gas: The ion current for group 3 was lower by one order of magnitude then that of other groups; however, all groups were well within specification limits.

Tests No. 7, 8, 9.--Ten cycles of -55 to 100°C and then measurement of gas: Data for groups 1 and 2 were comparable and of low value of ion current. Group 3 data showed excessively high ion current in three bottles after one of the temperature shock cycles, which in one bottle diminished after a later cycle and increased after a subsequent cycle. However, all values were within the specifications value of 1×10^{-6} A.

Test No. 10.--Humidity test for 3 days and then measurement of gas: Groups 1 and 2 had very low values of ion current, well within specifications. Group 3 was like the other groups, except that one sample had ion current nearly two orders of magnitude higher than those of the other samples.

It was concluded that group 1 samples were the most consistent and within specifications and, therefore, would offer the highest production yield. For the first article sample evaluation, GE fabricated four each of group 1 vacuum envelopes.

Because of the out-of-specifications ion current after seal off of the samples, the exhaust schedule was changed. During fabrication of these later samples, the schedule was modified to keep the filament hot after seal off as the vacuum bottles were cooling to 300°C. This heat allowed any residual gas to be gettered by the Nb rather than by the filaments.

All samples produced met all specification requirements, so the group 1 design will probably meet the long-term requirements for permeation. However, there is not adequate evidence that the design is any better than existing designs with respect to microcracking and outgassing of initially trapped gas.

With respect to these uncertainties, the group 1 design is being evaluated further in the HDL Surveillance Test Program. The following samples will be systematically tested and evaluated over a minimum of 5 yr:

17 group 1 vacuum bottles
12 group 1 bottles in cavities
8 group 1 A2 devices

5. DISCUSSION

5.1 Leaking

All experimenters observed incidences in which catastrophic failure of the A2 vacuum bottles occurred because microcracks propagated completely through the ceramic. This type of failure causes a real leak, and the vacuum bottle reaches atmospheric pressure quickly. Although this failure mode occurs frequently during experimental testing and disassembly, the HDL failures were not believed to be due to leaks. Those failures are of basically three types: (1) A spike type of ion-current trace quickly cleaned up (fig. 26) and showed monotonic increase over monitoring periods of as much as 1 yr. (2) A peak ion-current trace had less rapid cleanup (fig. 27). (3) A combination of spike and peak ion-current traces is shown in figure 28. A real leak would characteristically be expected to exhibit a monotonic increase in ion current with time

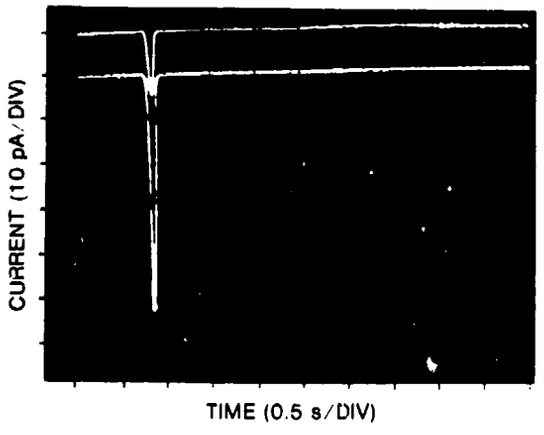

Figure 26. Spike type of ion current.

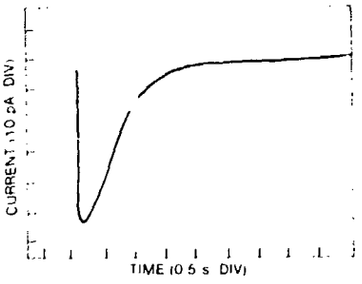

Figure 27. Peak ion current.

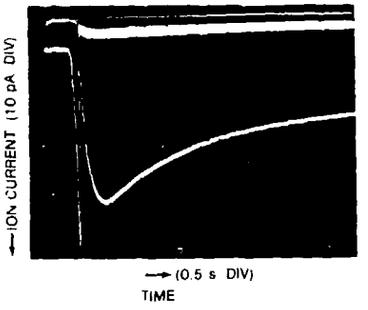

Figure 28. Combination of spike and peak ion current.

until atmospheric pressure would be reached. At HDL, ion-current data have accumulated on hundreds of A2 devices whose ages range from a few months to several years. All ion currents on these devices are less than 10^{-2} A and show no evidence of additional gas up, but show declining ion current with successive measurements. This decline is very uncharacteristic of leaks.

At NRL, gas in a variety of bad tubes was examined. Oxygen was not found in any vacuum tube; thus, outside air could not have entered the tube. Sandia reported the presence of O_2 in one sample; HDL and the failure-analysis team unanimously believed that the leak was caused by vacuum-bottle preparation. This belief is supported by the following facts:

a. From 7 November 1973 until 21 February 1974, the maximum pressure monitored was 8×10^{-10} Torr.

b. Assume a leak flow rate of 10^{-13} Torr liter/s (the minimum leak that Sandia can detect). The tube volume is 0.0005 liter, and t = time required to reach 10^{-4} Torr; then

$$t = \frac{10^{-4} \times 0.0005}{10^{-13}} = 5 \times 10^{5} \text{ s} .$$

Thus, t is less than 1 wk. Sandia checked the tube approximately 10 months after HDL's final ion-current test and reported that it had a pressure of 303 Torr. This pressure means that the tube total pressure increased more than six orders of magnitude after the device left the control of HDL.

At ECOM, the braze regions from many samples were reported satisfactory. The failure-analysis team, however, advised that reactive metal seals should not be used. The basic reason is that the Ti in the

active seals adsorbs gas during the sealing process. Thus, when the predetermined eutectic temperature is reached, melting may have already occurred, since some Ti would have been converted to oxides and nitrides. As a result, the amount of Ti available to form the alloy is variable, the eutectic melting point is unpredictable, and seals are unreliable.

The anode/cathode spacer is the highest stressed ceramic in the tube. Consequently, if a material's coefficient of expansion were matched with that of the ceramic, a more reliable seal would result. The failure-analysis team suggested that Mo is a much closer match of expansion with the ceramic than Cu, and thus seals made with Mo are in compression at the time that they are formed. This better matching results in a very thin layer of braze material and a more reliable seal.

5.2 Permeation

The most common gas for permeation, H_2, has its greatest permeation through metals, while He has its greatest through electrical insulating materials. It is assumed that high-alumina ceramic is impermeable to He. Also, both NRL and Sandia independently observed that He was not one of the residual gases in bad vacuum bottles. Therefore, all the permeation work reported here is limited to H_2.

Sandia and NRL report the presence of H_2 in various amounts in all tubes analyzed. This H_2 was assumed to have come from the H_2 in the atmosphere via permeable materials in the vacuum envelope. If this assumption were valid, and since the partial pressure of H_2 in the atmosphere is 4×10^{-4} Torr, a serious vacuum degradation problem might be expected due to permeation.

Sandia's calculations revealed that the A2 vacuum envelope contains permeable materials. In particular, Sandia's calculations can be interpreted to mean that if A2 assemblies containing clean Nb were exposed to the atmosphere at room temperature, the vacuum inside would remain for 75 days. Later, the pressure inside would rise to 4×10^{-4} Torr in 4 hr. All A2 assemblies are exposed to this environment, but for the majority of items examined, pressure rises of this magnitude and in this time frame have not been observed.

The failure analysis team has considered the question of why the calculations differ from real life and suggests the following explanation: When clean Nb is exposed to atmospheric gases, it immediately reacts with the O_2 in the atmosphere to form an oxide coat. This coat acts as a permeation barrier that precludes or significantly reduces permeation rates In addition, the permeation calculations were made for a 0.1-cm^3 volume, whereas the actual volume is 0.5 cm^3.

The greatest permeability of the vacuum bottle has been to atomic H. Atomic H does not exist in the atmosphere, but vacuum degradation might occur if it could be produced artificially at the Nb surface of the bottle envelope. The penetration of the Nb envelope by H is less difficult than by H_2.

Sandia studied the problem of H evolution from room-temperature vulcanization (RTV) silicones similar to those used as potting material from the A2 vacuum bottles. This study examined H evolution from several RTV silicones and concluded that with the exception of the GE 511 type, all of them evolved H to some degree. The consensus of the team was that the levels of evolved H from RTV silicones examined were insignificant and that further investigation was not required.

General Electric observed that significant increases in ion current occurred on many GE vacuum devices after exposure to combinations of high temperature (75°C) and high humidity (95 percent). This observation was interpreted GE to mean that the devices were permeable, and this permeability was caused by the Nb used in the vacuum-envelope construction. So convincing was this observation that GE eliminated Nb from the vacuum envelope and manufactured a sizeable quantity of these new devices. But they could not be marketed since most, if not all, of them showed H spikes that exceeded the HDL specification of 10^{-8} A after a 30-day holding period. This result proves conclusively that the H observed in these devices was not via permeation through the Nb in the vacuum envelope.

It is now known that the thoriated tungsten (W) filament can act as a source of H. The temperature gradient of the filament during operation is such that a portion of the filament ranges from 200° to 500°C. In this temperature range, the filament becomes a very efficient getter. It is postulated that the H spikes reported by GE were in fact caused by H that would have initially been trapped by Nb, but was instead trapped by the filament. In time, this trapped gas diffused up the filament at a point where it could be subsequently released when the filament was energized.

Boyd reported (unpublished) that H_2 contamination of a filament might occur during the filament carburization process. Boyd constructed tubes using filaments that were not carburized in an H_2 atmosphere. Boyd reported that the residual pressure in this tube at seal off was two orders of magnitude less than some tubes made with filaments carburized in an H_2 atmosphere.

5.3 Outgassing

All materials give off gas to some extent when heated. Because they do, all materials used in vacuum-tube construction are baked at

temperatures as high as 1000°C. In spite of this heat, when the final vacuum seal is made, gas is trapped inside the vacuum envelope. Early in the A2 device investigation, HDL limited the pressure at seal off, as indicated by ion current, to 10^{-6} A. This level is significantly less than the level required to cause deterioration at any of the critical tube parameters. Therefore, if all the initially trapped gas came out, A2 device performance would not be compromised. Some bad tubes have indicated ion current readings of several orders of magnitude greater than the 10^{-6} A allowed at tube seal off. In these tubes, it is clear that the vacuum degradation observed is caused by something other than the outgassing of initially trapped gases.

5.4 Microcracks

Cracks were observed in all ceramics of all tubes examined, both good and bad. How, then, can microcracking explain the observed vacuum degradation that occurs in only approximately 10 percent of the A2 devices produced?

All A2 vacuum bottles examined had cracks at internal bottle surfaces. The examination could not determine when these cracks occurred. If they occurred before the final seal was made at the vacuum system, then no gas-up problem could occur. If the cracks occurred during factory processing, the manufacturer could bury these gases by dc and rf cleanup methods. Microcracks would be detected as gas failures if they occurred after HDL received the A2 devices. Such failures might occur as a result of crack propagation. Vacuum bottles in cavities were subjected to thermal shock and showed that the average crack length and the number of pores intercepted were higher than in similar devices that had not been shocked.

The high stresses reported earlier are relieved partially during factory processing; thus, stable equilibrium of the remaining stresses exists at room temperature. The magnitude of the remaining stresses is subject to statistical variation that depends primarily on the thermal history of the particular A2 vacuum bottle. These existing stresses are further relieved by propagation of existing microcracks. Tests conducted by PA clearly show that tubes with low initial gas readings can be made to exhibit very large ion-current readings by subjecting the assemblies to severe temperature shock cycles.

The propagation of such cracks should cause measurable acoustic emissions. However, after several attempts by two experimenters, propagating microcracks and simultaneous acoustic emissions and release of gas burst have not definitely been correlated. The overwhelming evidence is that vacuum degradation is caused by propagating microcracks. These cracks erupt gas-filled pores in the ceramic. Seven facts have definitely been established:

a. Calculated stresses in the ceramic are at or near the fracture stress of the ceramic.

b. Cracks in the ceramic have been observed on numerous occasions, and the origins of the cracks correspond to the calculated points of maximum stress.

c. The direction of crack propagation is commonly observed to be away from the inside wall and, hence, in the proper direction to connect voids within the wall to the interior of the tube.

d. The ceramic contains pores of gas, mainly N_2. The residual gas in bad tubes is mainly N_2.

e. The propagation of cracks in a piece of ceramic from bad tubes leads to an increase in N_2 pressure approaching 10^{-2} Torr.

f. A few severe thermal shocks cause significant gas increases in most samples.

g. Ion-current data on hundreds of bad tubes indicate that the majority of the bad items checked, after more than 1-yr storage, indicated initial high ion-current readings. But subsequent readings continued to decline, indicating that the gas source was depleted. Such gas-ion-current behavioral characteristics with time might be expected when the gas buildup phenomenon is caused by release of gas from pores that were opened by a propagating microcrack system.

6. CONCLUSION

Degradation of most A2 vacuum tubes is caused by the release of gas into the tubes from pores in the ceramic that were ruptured by propagating microcracks and, in some tubes, by the thermal desorption of gases that were trapped in the filament during filament or A2 vacuum tube processing.

7. RECOMMENDATIONS

From this study have come five recommendations:

a. Eliminate active metal seals by using molymanganese metallized ceramic seal faces and ductile brazing alloys. This elimination will result in a low-stress system; thus, the probability of microcracks being produced will be reduced.

b. Eliminate Ag-bearing alloys in the final vacuum seal. Experiments have shown that Ti-Ag alloys used in some of the fielded devices corrode when exposed to extended periods at high humidity and high temperature. An Ni-Cu-Au alloy (NIORO) is superior to the Cu-Ag used by some A2 vendors.

c. Since calculations have shown that Nb is the most permeable material used in the vacuum envelope, eliminate or use Nb in a manner that will not provide a permeable path into the vacuum envelope. Replace Nb and buttons with Mo, and use a getter material to compensate for the gettering action of the Nb. Titanium outgasses H_2 from 200° to 900°C and, therefore, should be thoroughly outgassed before use.

d. Filament carbonization (covering the filament surface with a thin layer of C) is done in an H_2 atmosphere. The H_2 contamination of the filament cannot be avoided. To purge the filaments of this H_2 as well as other gases, the filaments should be operated before and after the exhaust cycle. Operating the filament before final exhaust allows desorbed gases to be removed by the vacuum pump. Operation of the filaments during cooling does not allow the filaments to getter. From 200° to 500°C, cooling should be rapid to minimize the time during which the filaments are at these temperatures. Thoriated W filaments getter gas efficiently in this temperature range.

e. The A2 device surveillance plan should be continued, and the acceptance levels should be increased. The present specification of 2.10^{-9} A/month change is based on reaching a final pressure after 10 yr of $2.10^{-9} \times 12 \times 10$ A = 1.2×10^{-7} A. This level of gas is three orders of magnitude below the level where A2 malfunction might be expected to occur.

f. A higher tensile strength ceramic should be used in new vacuum bottles. Microcracking occurs because the residual stresses set up during the braze cycle approach the tensile strength of the present ceramic. The probability of microcracking would thus be reduced for higher-tensile-strength ceramic.

ACKNOWLEDGEMENT

The following researchers comprised the failure-analysis team: Edward J. Cook of ADL Co.; Bruce Barnaby of Sandia; Roy Rice, George Haas, Henry Gray, and Stephen Freiman of NRL; Nelson Wilson, Joel Shappiro, and Charles F. Cook, Jr., of ECOM; Sheldon Wiederhorn of NBS; Dennis Viechnicki of AMMRC; Augustine Magistro, Louis DeVaughn, John Kuchmas, and A. Graph of PA; Stanley F. Kaisel, consultant; and Horst Gerlach, Walter Hattery, William E. Isler, Bruce E. Lackey, Charles Marshburn, Charles M. Quicke, Dale Schroeder, and Joseph Tokarcik of HDL.

DISTRIBUTION

DEFENSE DOCUMENTATION CENTER
CAMERON STATION, BUILDING 5
ALEXANDRIA, VA 22314
ATTN DDC-TCA (12 COPIES)

COMMANDER
USA RSCH & STD GP (EUR)
BOX 65
FPO NEW YORK 09510
ATTN LTC JAMES M. KENNEDY, JR.
CHIEF, PHYSICS & MATH BRANCH

COMMANDER
US ARMY MATERIEL DEVELOPMENT
& READINESS COMMAND
5001 EISENHOWER AVENUE
ALEXANDRIA, VA 22333
ATTN DRXAM-TL, HQ TECH LIBRARY
ATTN DRCDE, DIR FOR DEV & ENGR
ATTN DRCDE-E, SPECS, STDS, & ENGR
ATTN DRCSF-N, NUCLEAR

COMMANDER
USA ARMAMENT COMMAND
ROCK ISLAND, IL 61201
ATTN DRSAR-ASF, FUZE DIV
ATTN DRSAR-RDF, SYS DEV DIV - FUZES
ATTN DRSAR-PDS, ENGR SUPPORT DIV

COMMANDER
USA MISSILE & MUNITIONS CENTER & SCHOOL
REDSTONE ARSENAL, AL 35809
ATTN ATSK-CTD-F

US DEPARTMENT OF COMMERCE
NATIONAL BUREAU OF STANDARDS
WASHINGTON, DC 20230
ATTN DR. SHELDON WIEDERHORN

COMMANDER
US ARMY ELECTRONICS COMMAND
FT. MONMOUTH, NJ 07703
ATTN DRSEL-SA, SYS ANALYSIS OFC
ATTN DRSEL-RD, DIR, RES, DEV, & ENGR
ATTN DRSEL-CT-D, COMBAT SURVEILLANCE
& TARGET ACQUISITION
ATTN MR. NELSON WILS
ATTN DR. JOEL SHAPPI
ATTN MR. CHARLES CO

COMMANDER
US ARMY MATERIALS & MECHANICS
RESEARCH CENTER
WATERTOWN, MA 02172
ATTN DRXMR-H, BALLISTIC MISSILE DEF
MATERIALS PROGRAM OFC
ATTN TECHNICAL LIBRARY
ATTN DR. DENNIS VIECHNICKI

COMMANDER
US ARMY MATERIALS SYSTEMS
ANALYSIS ACTIVITY
ABERDEEN PROVING GROUND, MD 21005
ATTN DRXSY-CC, COMM & ELECTRONICS

COMMANDER
US ARMY MATERIEL DEVELOPMENT AND
READINESS COMMAND
LETTERKENNY ARMY DEPOT
CHAMBERSBURG, PA 17201
ATTN DRXLS, DARCOM LOGISTIC SYS
SUPPORT AGENCY

PROJECT MANAGER, LANCE
US ARMY MATERIEL DEV AND
READINESS COMMAND
REDSTONE ARSENAL, AL 35809

PROJECT MANAGER, SAM-D
US ARMY MATERIEL DEV &
READINESS COMMAND
REDSTONE ARSENAL, AL 35809

COMMANDER
US ARMY MISSILE COMMAND
REDSTONE ARSENAL, AL 35809
ATTN DRCPM-HA, OFC PROJ MNGR, HAWK
ATTN TECHNICAL LIBRARY

US ARMY MISSILE RESEARCH, DEV, &
ENGINEERING LABORATORY
US ARMY MISSILE COMMAND
REDSTONE ARSENAL, AL 35809
ATTN DRSMI-RB, REDSTONE SCI INFO
CTR (2 COPIES)

COMMANDER
US ARMY NATICK RES & DEV COMMAND
US ARMY NATICK DEVELOPMENT CENTER
NATICK, MA 01760
ATTN DRXNM-E, ENGR PROG MNGMT OFC

COMMANDER
REDSTONE SCIENTIFIC INFORMATION CENTER
US ARMY MISSILE COMMAND
REDSTONE ARSENAL, AL 35809

COMMANDER
WHITE SANDS MISSILE RANGE, NM 88002
ATTN STEWS-TE, ARMY MISSILE TEST &
EVALUATION DIV

COMMANDER
FRANKFORD ARSENAL
BRIDGE & TACONY STREETS
PHILADELPHIA, PA 19137
ATTN L1000, PITMAN-DUNN LABORATORY
CHIEF OF RES DIV
ATTN K1000, TECH LIB

DISTRIBUTION (Cont'd)

COMMANDER
HQ, PINE BLUFF ARSENAL
PINE BLUFF, AR 71601
ATTN SARPB-ET, DIR OF ENGR & TECH

COMMANDER
PICATINNY ARSENAL
DOVER, NJ 07801
ATTN SARPA-AD-F, FUZE DEV & ENG DIV
ATTN SARPA-ND, NUCLEAR DEV & ENGR DIR
ATTN SARPA-ND-S, SYSTEMS ENGR DIV
ATTN SARPA-ND-D-B, MR. AUGUSTINE MAGISTRO
ATTN SARPA-ND-E-A, MR. LOUIS DEVAUGHN
ATTN SARPA-FR-S-P, MR. AL GRAF (5 COPIES)
ATTN SARPA-FR-S-P, MR. JOHN KUCHMAS

COMMANDER
ROCK ISLAND ARSENAL
ROCK ISLAND, IL 61201
ATTN SARRI-LE, APPLICATION ENGR DIR

COMMANDER
WATERVLIET ARSENAL
WATERVLIET ARSENAL, NY 12189
ATTN SARWV-RDD, DEV ENGR DIR

DIRECTOR
NAVAL RESEARCH LABORATORY
WASHINGTON, DC 20375
ATTN CODE 2620, LIBRARY (2 COPIES)
ATTN CODE 5230, DR. GEORGE HASS (3 COPIES)
ATTN CODE 5230, DR. HENRY GRAY
ATTN CODE 6360, MR. ROY RICE
ATTN CODE 5230, DR. SHEPHAN FREIMAN
ATTN CODE 5230, MR. RICHARD THOMAS

COMMANDER
NAVAL SURFACE WEAPONS CENTER
WHITE OAK, MD 20910
ATTN WA-05, FUZE PROGRAM MANAGER
ATTN WA-30, RADAR & FUZING DIV
ATTN WA-33, FUZING BR

COMMANDER
NAVAL WEAPONS CENTER
CHINA LAKE, CA 93555
ATTN CODE 3007, WEAPONS SYS ANAL
ATTN CODE 40, WEAPONS DEV DEPT
ATTN CODE 50, FUZE DEPT
ATTN CODE 533, TECHNICAL LIBRARY

ASSISTANT SECRETARY OF THE AIR FORCE
(RESEARCH & DEVELOPMENT)
WASHINGTON, DC 20330

COMMANDER
AEROSPACE RESEARCH LABORATORIES
WRIGHT-PATTERSON AFB, OH 45433
ATTN LL, METALLURGY & CERAMICS RES

DIRECTOR
AF AVIONICS LABORATORY
WRIGHT-PATTERSON AFB, OH 45433
ATTN RWA, ANALYSIS & EVAL BR

COMMANDER
AF EASTERN TEST RANGE (AFSC)
PATRICK AFB, FL 32925
ATTN SEA, MISSILE FLIGHT ANALYSIS

DIRECTOR
AF MATERIALS LABORATORY
WRIGHT-PATTERSON AFB, OH 45433
ATTN LL, METALS & CERAMICS DIV
ATTN JOE MEULEMANN

COMMANDER
HQ ROME AIR DEVELOPMENT CENTER (AFSC)
GRIFFISS AFB, NY 13441
ATTN OC, SURVEILLANCE DIV

DIRECTOR
AF OFFICE OF SCIENTIFIC RESEARCH
1400 WILSON BLVD
ARLINGTON, VA 22209
ATTN NM, DIR OF MATHEMATICAL
& INFO SCI

COMMANDER
HQ AIR FORCE SYSTEMS COMMAND
ANDREWS AFB
WASHINGTON, DC 20331
ATTN TECHNICAL LIBRARY

ESTERLINE ELECTRONICS CORPORATION
3501 N. HARBOR BLVD
COSTA MESA, CA 92626
ATTN MR. GEORGE WELLS
ATTN MR. JOHN HENDRICKSON
ATTN MR. THOMAS BURTON, HDL REP

ARTHUR D. LITTLE COMPANY
25 ACORN PARK
CAMBRIDGE, MA 02140
ATTN DR. EDWARD J. COOK

SANDIA CORPORATION
VACUUM TUBE DIVISION, 2414
ALBUQUERQUE, NM 87101
ATTN MR. BRUCE BARNABY

DR. STANLEY F. KAISEL
P.O. BOX 4153
WOODSIDE, CA 94062

MR. CHARLES E. MARSHBURN
21142 STRATHMOOR LANE
HUNTINGTON BEACH, CA 92646

DISTRIBUTION (Cont'd)

HARRY DIAMOND LABORATORIES
ATTN MCGREGOR, THOMAS, COL, COMMANDER/
FLYER, I.N./LANDIS, P.E./
SOMMER, H./OSWALD, R. B.
ATTN CARTER, W.W., DR., TECHNICAL
DIRECTOR/MARCUS, S.M.
ATTN KIMMEL, S., PAO
ATTN CHIEF, 0021
ATTN CHIEF, 0022
ATTN CHIEF, LAB 100
ATTN CHIEF, LAB 200
ATTN CHIEF, LAB 300
ATTN CHIEF, LAB 400
ATTN CHIEF, LAB 500
ATTN CHIEF, LAB 600
ATTN CHIEF, DIV 700
ATTN CHIEF, DIV 800
ATTN CHIEF, LAB 900
ATTN CHIEF, LAB 1000
ATTN RECORD COPY, BR 041
ATTN HDL LIBRARY (3 COPIES)
ATTN CHAIRMAN, EDITORIAL COMMITTEE
ATTN CHIEF, 047
ATTN TECH REPORTS, 013
ATTN PATENT LAW BRANCH, 071
ATTN GIDEP OFFICE, 741
ATTN LANHAM, C., 0021
ATTN GERLACH, HORST, W. A., 110
ATTN CHIEF, BR 110
ATTN HATTERY, W., 130
ATTN ISLER, W. E., 950
ATTN TOKARCIK, J. J., 750 (10 COPIES)
ATTN QUICKE, C., 740
ATTN WILLIS, B. F., 740 (2 COPIES)
ATTN SCHROEDER, D., 722
ATTN MCNEIL, W. K. (5 COPIES)